

THROUGH-THICKNESS REINFORCEMENT FOR WOVEN LAMINATES

ALEJANDRA G. CASTELLANOS

Master's Program in Mechanical Engineering

APPROVED:

Pavana Prabhakar, Ph.D., Chair

Yirong Lin, Ph.D.

David A. Roberson, Ph.D.

Charles Ambler, Ph.D.
Dean of the Graduate School

©Copyright

by

Alejandra G. Castellanos

2016

*to my
Family and Friends
with unconditional love*

THROUGH-THICKNESS REINFORCEMENT FOR WOVEN LAMINATES

by

ALEJANDRA G. CASTELLANOS

THESIS

Presented to the Faculty of the Graduate School of

The University of Texas at El Paso

in Partial Fulfillment

of the Requirements

for the Degree of

MASTER OF SCIENCE

Department of Mechanical Engineering

THE UNIVERSITY OF TEXAS AT EL PASO

May 2016

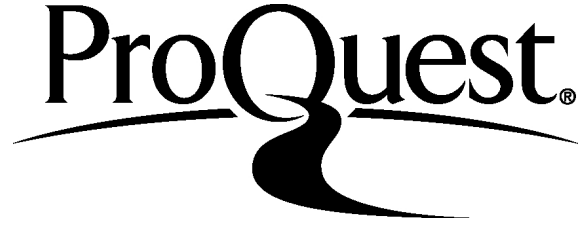
ProQuest Number: 10118238

All rights reserved

INFORMATION TO ALL USERS

The quality of this reproduction is dependent upon the quality of the copy submitted.

In the unlikely event that the author did not send a complete manuscript and there are missing pages, these will be noted. Also, if material had to be removed, a note will indicate the deletion.



ProQuest 10118238

Published by ProQuest LLC (2016). Copyright of the Dissertation is held by the Author.

All rights reserved.

This work is protected against unauthorized copying under Title 17, United States Code
Microform Edition © ProQuest LLC.

ProQuest LLC.
789 East Eisenhower Parkway
P.O. Box 1346
Ann Arbor, MI 48106 - 1346

Acknowledgements

I would like to express my deep-felt gratitude to my advisor, Dr. Pavana Prabhakar from the Mechanical Engineering Department at The University of Texas at El Paso, for her advice, encouragement, enduring patience and constant support through my master.

I also wish to thank the other members of my committee, Dr. Yirong Lin from the Mechanical Engineering Department and Dr. David Roberson from the Metallurgical, Materials and Biomedical Engineering Department, both from The University of Texas at El Paso for their guidance and expertise I needed in order to complete this work.

I want also to thank Shuvo, Jerry, Jose and Emilio for the ZnO nanowires. I want to thank Andy for his unconditional love and support during my master. Andy, thanks to you I am here. Additionally, I want to thank all my friends who have been in every step of my educational process and who have give me all kind of support (not in specific order): Luis Chavez, Diego Delfin , Luis Varela, Luz Bugarin, Raudel Avila, Luis Delfin, Daniela Aguilar, Juan Gomez, Alan Esparza, Jesus Ortega, Ricardo Martinez, Armando Delgado, Sergio Guerrero, Jerry Rodriguez, Sergio Quevedo, Jaime Cruz, Jose Romero and Marco Avalos. Thank you guys for all your support and never letting me quit, without you it would not be the same. I love every one of you.

Abstract

Fiber reinforced polymer composites have gained popularity in aerospace and naval applications due to their tailorable mechanical properties and high strength-to-weight. Despite these advantages, between the layers of fabric (laminas), there is a resin-rich region known as interlaminar region, with no reinforcement which is very susceptible to damage. Different types of reinforcements have been tested for the interlaminar region. However, all of these methods have proved to decrease the in-plane properties due to damage to the fibers. In this thesis, a new reinforcement technique with ZnO nanowires is proposed to increase the damage resistance. This thesis describes the design, manufacturing and testing of woven composites with ZnO nanowire reinforcement. Damage resistance and durability of these composites are evaluated under quasi-static loading (Mode-I and Mode-II) and under dynamic loading (impact). Nanowire reinforcements appear to increase the damage resistance of a composite without reducing the in-plane properties of the composite. For quasi-static loading, the improvement of the interlaminar fracture toughness for Mode-I and Mode-II was approximately 74% and 28%, respectively. For dynamic loading, the damage degree was reduced by approximately 18%. This improvement is attributed to the resistance of nanowire reinforcement towards creating new surfaces.

Table of Contents

	Page
Acknowledgements	v
Abstract	vi
Table of Contents	vii
List of Tables	ix
List of Figures	x
Chapter	
1 Introduction	1
1.1 Materials	2
1.1.1 Matrix Phase	2
1.1.2 Reinforcing Phase	4
1.2 Manufacturing Process	5
1.2.1 Hand Lay-up	5
1.2.2 Compression Molding	6
1.2.3 Resin Transfer Molding	6
1.2.4 Filament Winding	7
1.2.5 Pultrusion	7
1.2.6 Prepreg	8
1.2.7 Vacuum Assisted Resin Transfer Molding	8
1.3 Fiber Reinforced Polymer Composites	9
1.4 Failure Mechanisms	9
1.5 Interlaminar Matrix Reinforcement	10
1.6 Scope and Outline of the Thesis	12
2 Nanowire Reinforcement of Woven Composites for Enhancing Interlaminar Fracture Toughness	13

2.1	Introduction	13
2.2	Manufacturing	15
2.2.1	VARTM Process for Composite Manufacturing	15
2.2.2	ZnO Nanowire Synthesis on Dry Fabric	17
2.3	Interlaminar Fracture Toughness	19
2.3.1	Mode-I Fracture Toughness: Double Cantilever Beam (DCB)	19
2.3.2	Mode-II Fracture Toughness: End-Notched Flexure (ENF)	20
2.4	Discussion of Results	22
2.4.1	Mode-I Fracture Toughness: Double Cantilever Beam (DCB)	22
2.4.2	Mode-II Fracture Toughness: End-Notched Flexure (ENF)	24
2.4.3	Fractographic Analysis	26
2.5	Conclusion	26
3	Interlaminar Reinforcement for Enhancing Low-Velocity Impact Response of Woven Composites	28
3.1	Introduction	28
3.2	Impact Modeling	30
3.3	Manufacturing	33
3.3.1	VARTM Process for Composite Manufacturing	33
3.3.2	ZnO Nanowire Synthesis on Dry Fabric	34
3.4	Impact Tests	36
3.5	Results and Discussion	37
3.6	Conclusion	40
4	Conclusion and Future Work	42
4.1	Conclusion	42
4.2	Major contributions	42
4.3	Future work	43
	References	44
	Curriculum Vitae	53

List of Tables

1.1	Properties of the most common thermoplastics	3
2.1	G_{IC} (kJ/m^2) without ZnO nanowires	24
2.2	G_{IC} (kJ/m^2) with ZnO nanowires	24
2.3	G_{IIC} (kJ/m^2)	26
3.1	Plain weave carbon lamina material constants [1]	31
3.2	Peak force, maximum deflection for samples with and without ZnO nanowires	37
3.3	Degree of damage	38

List of Figures

1.1	Phases of a composite	2
1.2	Schematics of different continuous fibers. (a)Unidirectional orientation; (b)bidirectional orientation; (c)random orientation.	5
1.3	Hand lay-up schematic	6
1.4	Compression molding schematic	6
1.5	RTM schematic	7
1.6	Filament winding schematic	7
1.7	Filament winding schematic	8
1.8	Vacuum assisted resin transfer molding schematic	8
1.9	Fiber reinforced polymer composites	9
1.10	Failure mechanisms: (a) fiber fracture (Scale: 500 μm); (b) micro-cracks in matrix (Scale: 500 μm); (c) fibers-matrix debonding (Scale: 30 μm); (d) fiber pullout (Scale: 500 μm); (e) delamination (Scale: 500 μm)	10
1.11	Through-thickness reinforcement: (a) stitching; (b) 3D weaving; (c) z- pinning; (d) carbon nanotubes (CNTs)	11
2.1	(a) VARTM configuration for the 2D carbon woven composite; (b) Laminate preparation in progress using VARTM process	16
2.2	(a) Teflon sheet insert to simulate a crack for DCB sample; (b) Teflon sheet insert to simulate a crack for ENF sample	17
2.3	ZnO nanowires grown on 2D woven carbon fiber at different scale a) 1 mm, b) 40 μm and c) 5 μm	18
2.4	Sample dimensions for DCB test	20
2.5	DCB test in progress of a carbon fiber laminate with ZnO nanowires	21
2.6	Sample dimensions for ENF test	21
2.7	ENF test in progress of a carbon fiber laminate with ZnO nanowires	22

2.8	Typical load-displacement response of a DCB test specimen without nanowires	23
2.9	Typical load-displacement response of a DCB test specimen with nanowires	23
2.10	Load-displacement response for specimens without nanowires for ENF . . .	25
2.11	Load-displacement response for specimens with nanowires	25
2.12	(a) Fracture surface for a specimen with ZnO nanowires (Scale: 1 mm); (b) Fracture surface for a specimen without ZnO nanowires (Scale: 1 mm); (c) Fracture surface for a specimen with ZnO nanowires (Scale: 500 μm); (d) Fracture surface for a specimen without ZnO nanowires (Scale: 500 μm); (e) Fracture surface for a specimen with ZnO nanowires (Scale: 100 μm); (f) Fracture surface for a specimen with ZnO nanowires (Scale: 100 μm) . . .	27
3.1	Schematic of fabric layers and interlaminar regions of the laminate	30
3.2	(a) Impact model of specimen with boundary conditions; (b) Meshed elements using C3D8R elements	31
3.3	Contact force versus time of the impact model	32
3.4	Interlaminar regions that exhibit higher stresses	33
3.5	VARTM configuration for the carbon woven composite	34
3.6	Schematic of a 12 in. by 12 in. laminate manufactured	34
3.7	ZnO nanowires grown on 2D woven carbon fiber at different scale: a) 1 mm, b) 40 μm and c) 5 μm	35
3.8	(a) Specimen dimensions; (b) Impact fixture schematic	36
3.9	Normalized force-time response for energies of 2, 5, 10, 20 and 25J	37
3.10	(a) Energy vs time graph; (b) Definition of degree of damage	38
3.11	Images of the cross-section of the laminate impacted ar 10J. (a)Laminate without ZnO nanowires; (b)Laminate with ZnO nanowires.	39
3.12	Images of top impacted layer, bottom layer and cross-section of the specimens with and without ZnO nanowires impacted at 25 J.	40

Chapter 1

Introduction

Technology is improving every day; as a result, human beings have become more demanding. They want the lightest cell phones, the car with the best fuel efficiency and the fastest computer. Most of these innovations have been possible due to advancements in the field of materials. Although technology is evolving, materials are not at the same rate. To overcome this problem, materials like polymers, composites, and ceramics have become a very attractive option to replace conventional materials such as steel and aluminum. Composite materials are not an invention of human kind, as they exist in nature. A perfect example is wood, which is made by cellulose fibers that are held together in a substance known as lignin [2]. Cotton is also made by cellulose fibers, but the combination of cellulose fibers with lignin, which is weaker than cellulose fibers, is what makes wood stronger than cotton. Composite materials are not a new technology as they were used thousands of years ago. The first register of humankind using composites was from ancient Egypt. Egyptians used chopped straw to reinforce mud bricks and laminated wood veneer reinforcing with glue for sarcophagi. Later, metals started to dominate the world. First bronze in 1500 BC, then iron, and steel in 1850 [3]. Composite materials then began to gain popularity again in 1980 due to their excellent mechanical properties [4]. Composite materials are a combination of two or more constituent materials with different mechanical properties. This combination results in a "super" material that exhibits the best properties of the constituent materials plus added properties that the individual materials do not exhibit alone [5]. There are two general phases of constituent material: matrix phase and reinforcing phase (Fig. 1.1).

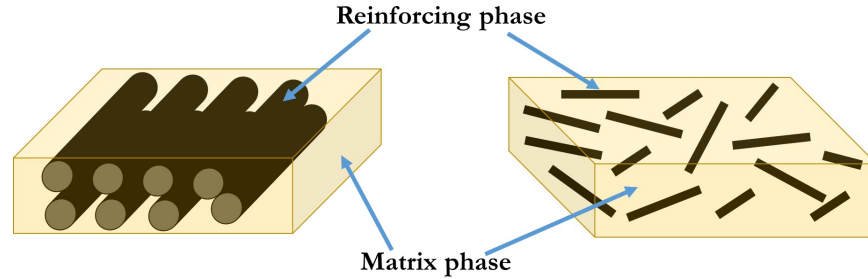


Figure 1.1: Phases of a composite

1.1 Materials

1.1.1 Matrix Phase

The matrix is a continuous phase which holds and transfers loads to the reinforcing phase [6]. The matrix phase has very low mechanical properties compared to the reinforcing phase. However, the matrix phase has properties such as compressive strength, thermal resistance, and fatigue strength, which influences many mechanical properties of the overall composite [7]. The matrix phase could be a metal, a ceramic or a polymer.

Metal Matrix

There are three types of metal matrices: aluminum, magnesium and titanium. A metal matrix is chosen when improvement in wear, creep, and resistance to thermal distortion are needed in a composite. Unlike ceramic and polymer matrices, when reinforcement is added to metal matrices there is a small increase in stiffness [8].

Ceramic Matrix

The most common matrices are alumina (aluminum oxide) and alumino-silicate [9]. This matrix is chosen when improvement in hardness, high strength, chemical inertness, and low density are needed [7].

Polymer Matrix

Polymer matrix is called resin during manufacturing and matrix after curing. A polymer resin is mixed with a catalyst to begin the process of curing, in which the resin is solidified. This process can be exothermic or endothermic. The curing process can take minutes or hours, and it can take place at room or elevated temperatures, depending on the resin used [10]. There are two types of polymer matrices: thermoplastic and thermoset.

Thermoplastic matrices

While curing, these matrices do not go any chemical transformation [10]. The most common thermoplastic matrices are polyether ether ketone (PEEK), polyphenylene sulfide (PPS), polysulfone (PSUL), polyetherimide (PEI) and polyamide-imide (PAI) [11]. Table 1.1 shows the properties of each thermoplastic.

Table 1.1: Properties of the most common thermoplastics

Thermoplastics	Properties
PEEK	High fracture toughness Chemical resistance Wear resistance High temperature application Resistant to burning Low water absorption
PPS	Elevated temperature use Chemical resistance
PSUL	Stability under hot and wet conditions
PEI	Strength and stiffness at elevated temperatures Flame resistance
PAI	Chemical resistant properties High glass transition temperatures

Thermoset matrices

Thermoset resins are usually liquids or low melting point solids [11]. The most commonly used are polyester resins, epoxy resins, and vinyl ester resins. Thermoset resins are converted to a hard rigid solid after curing [12].

Polyester resins

These resins are easy to use and they have the lowest cost of resins available. The disadvantages are that the mechanical properties are moderate, and they have a high cure shrinkage [11].

Epoxy resins

These resins have high mechanical and thermal properties, have low shrinkage on curing and high water resistance [13]. The disadvantages are that epoxy resins are more expensive than vinyl ester resins and are very corrosive for handling [14].

Vinyl ester resins

Vinyl ester resins have high mechanical toughness, high chemical/environmental resistance and excellent corrosion resistance [11]. They are highly resistant to acids, alkalis, solvents, hypochlorite and peroxides [13].

1.1.2 Reinforcing Phase

The reinforcing phase is stronger and stiffer than the matrix. The role of this phase is to increment the mechanical properties of the composite. They are two types: particulate and fiber reinforcement.

Particulate Reinforcements

They can be spherical, platelets, or any other regular or irregular geometry [15]. Particulate composites tend to be much weaker and less stiff than fiber composites [16]. An example of a particulate composite is concrete. The particles can have random or with preferential orientation.

Fiber Reinforcements

Fiber reinforcements could be short (discontinuous) or long (continuous). Continuous fibers can be unidirectional (Fig. 1.2(a)), bidirectional (Fig. 1.2(b)) or random oriented (Fig. 1.2(c)). For easy handling, the fibers are arranged in layers of fabric known as lamina. Bidirectional laminas are made through different textile techniques such as braiding,

weaving, and knitting [17]. The most use bidirectional reinforcement is plain weave woven as shown in Fig. 1.2(b). Plain weave is made by interlacing warp yarns with weft yarns. The weft yarns correspond to the x-direction of the fabric and the warp yarns to the y-direction of the fabric. Each warp yarn crosses alternatively under and over each weft yarn [18]. This results in a multidirectional reinforce layer of fabric [19] in which cracks do not propagate due to the change of direction of the yarns. Woven laminas provide better strength and stiffness than unidirectional laminas. The most common used fibers are carbon, glass, aramid, polyethylene, polyester and nylon.

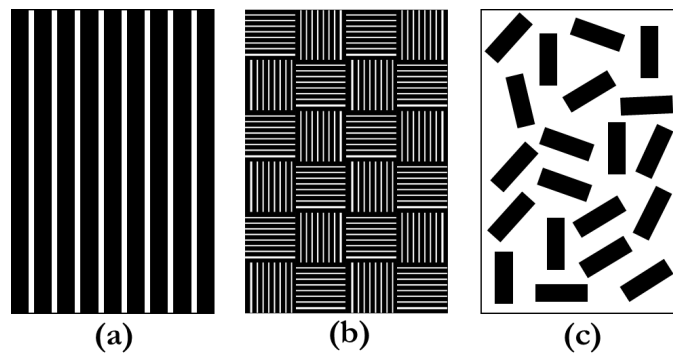


Figure 1.2: Schematics of different continuous fibers. (a) Unidirectional orientation; (b) bidirectional orientation; (c) random orientation.

1.2 Manufacturing Process

After selecting the matrix and reinforcement, the next step is the manufacturing process. The different manufacturing processes are described as follow:

1.2.1 Hand Lay-up

In this process, reinforcement and resin are placed in an open mold as shown in Fig. 1.3. The advantages of this process are low tooling cost, design flexibility, and no restriction on the size of parts to be fabricated [20]. The disadvantages are that the shape is limited to the mold use and that the product quality depends on operator skills [21].

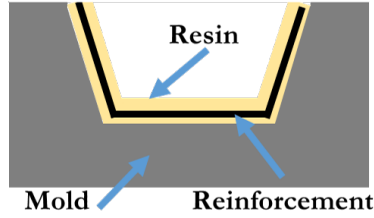


Figure 1.3: Hand lay-up schematic

1.2.2 Compression Molding

The layers of fabric and resins are subjected to a hydraulic pressure of up to 3000 psi in a mold, until the resin has cured [22] as shown in Fig. 1.4. The advantages of this system are that multiple parts can be manufactured in a single step, and it generates composite structures in less time [23]. The disadvantage is that the cost of processing is higher than other processes [23].

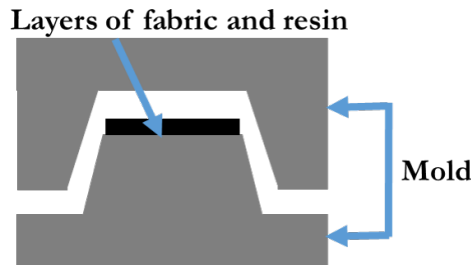


Figure 1.4: Compression molding schematic

1.2.3 Resin Transfer Molding

In this process, the layers of fabric are placed between closed molds as shown in Fig. 1.5. Resin is then pumped into the mold through injection ports [11]. The advantages are the low cost compared to other closed mold processes and the process is faster than hand lay-up [20]. The disadvantage is that the equipment needs is higher than hand lay-up.

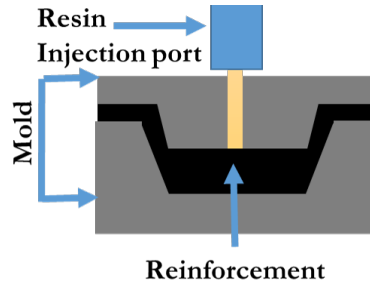


Figure 1.5: RTM schematic

1.2.4 Filament Winding

Fibers from a roving are bathed in resin, and then apply to a rotating mold surface (mandrel) to create cylindrical shapes as shown in Fig. 1.6. The advantages are that properties of the composite material can be controllable, different reinforcement and resin can be used, and the process can be highly automated [21]. The disadvantages are that it needs a rotating mold surface which can be expensive and that the fiber path cannot be changed easily [11].

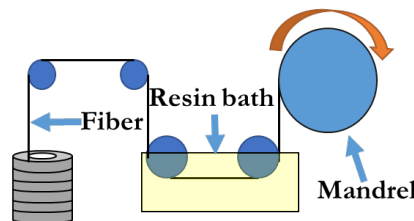


Figure 1.6: Filament winding schematic

1.2.5 Pultrusion

In this process, fibers are bathed in a thermoset resin bath. Then the fibers are shaped and heated to form a part as shown in Fig. 1.7. The advantages of this process are a very automated process, low labor content, and low cost of equipment and tooling compared to other high-volume composite processes [22]. The disadvantages are that the fibers have

very low strength in the transverse direction because the pultrudes orient the majority of the fibers in the tensile direction [11].

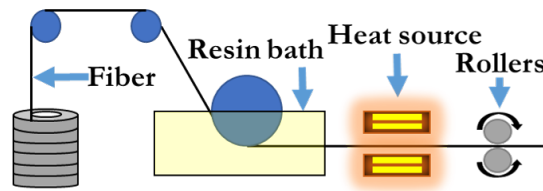


Figure 1.7: Filament winding schematic

1.2.6 Prepreg

In this method, layers of fabric are pre-impregnated with resin. No more resin is needed for manufacturing. The advantages are that there is less mess and less curing time for the laminate [7]. The disadvantages are the cost and the low shelf life of the prepregs [7].

1.2.7 Vacuum Assisted Resin Transfer Molding

In this method, dry layers of fabric are placed between two aluminum molds, followed by their enclosure in a vacuum bag as shown in Fig. 1.8. Vacuum is then used to aid the infiltration of the resin. After infusion, the resin is allowed to cure. The advantage of this process is that it creates a void-free laminate.

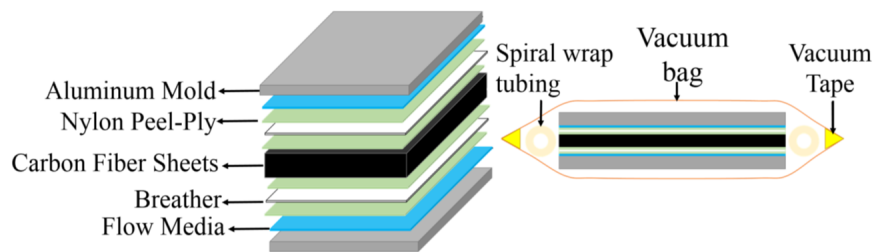


Figure 1.8: Vacuum assisted resin transfer molding schematic

1.3 Fiber Reinforced Polymer Composites

Fiber reinforced polymer (FRP) composites are used in aerospace vehicles, marine structures, and automobiles. FRP composites consist of layers of fabrics, known as laminas, reinforced in resin as shown in Fig. 1.9(a). A stack of laminas is known as laminate as shown in Fig. 1.9(b). This combination results in a material with high strength-to-weight ratio, tailorable mechanical properties, and corrosion and fatigue resistance. The mechanical properties along the fibers are strong and stiff. The region between the layers of fabric (Fig. 1.9(c)) is a resin-rich region known as interlaminar region. This region does not have any reinforcement, and it is very susceptible to damage, which can result in the premature failure of the composite [24, 25]. Most FRP composites fail due to the low mechanical properties of the resin.

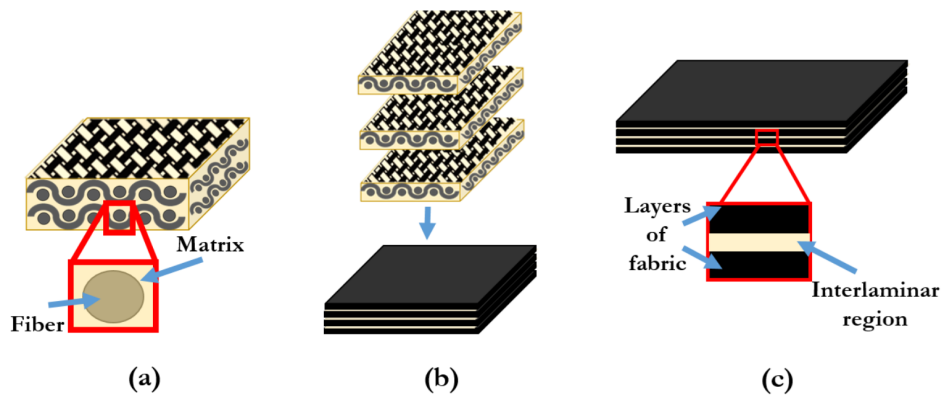


Figure 1.9: Fiber reinforced polymer composites

1.4 Failure Mechanisms

The life of a composite depends on its response to different failure mechanisms: fiber fracture (Fig. 1.10(a)), micro-cracks in matrix (Fig. 1.10(b)), debonding between fibers and matrix (Fig. 1.10(c)), fiber pullout (Fig. 1.10(d)), and delamination (Fig. 1.10(e)). Delamination is the separation of layers in a composite, and it is the most common failure mechanism. The propagation of delamination through the laminate is a combination of

normal and shear stresses [26]. To prevent or minimize the failure mechanisms, the damage tolerance of the laminate must be improved. A way of enhancing the damage tolerance is by improving the strength and toughness of interlaminar matrix regions. Strengthening this region improves the fracture toughness which increases the delamination resistance.

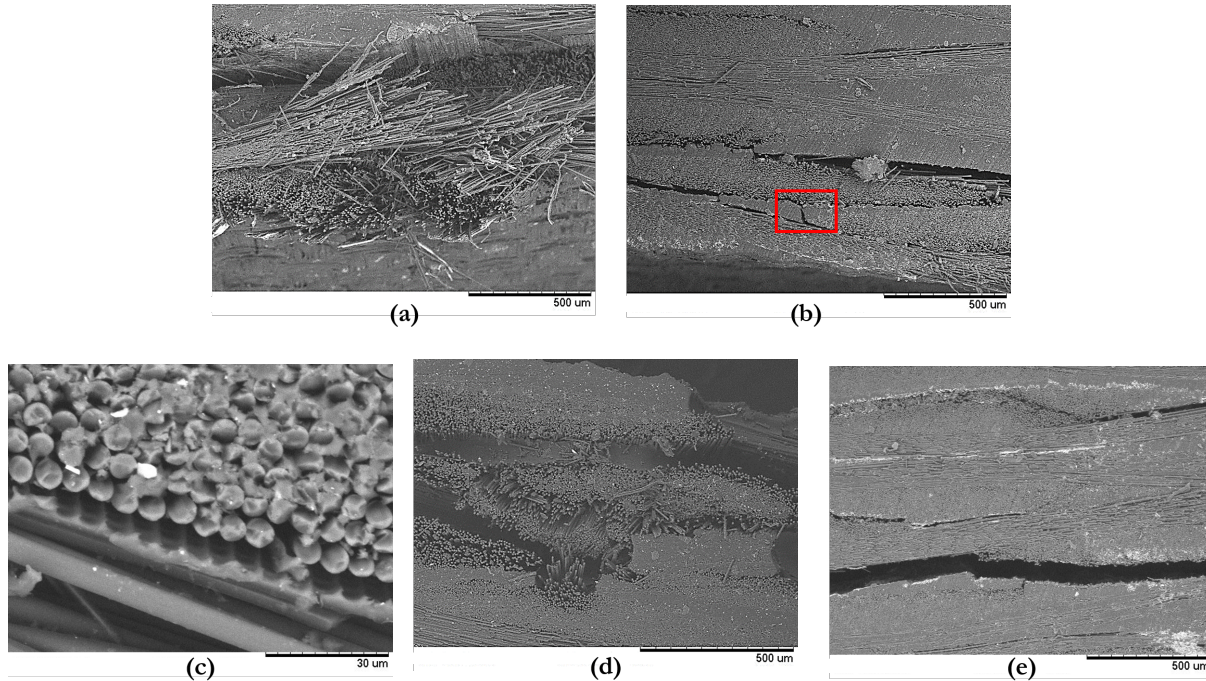


Figure 1.10: Failure mechanisms: (a) fiber fracture (Scale: 500 um); (b) microcracks in matrix (Scale: 500 um); (c) fibers-matrix debonding (Scale: 30 um); (d) fiber pullout (Scale: 500 um); (e) delamination (Scale: 500 um)

1.5 Interlaminar Matrix Reinforcement

FRP composites fail due to the lack of reinforcement in the interlaminar region. Several through-thickness reinforcements have been investigated by earlier research to prevent or minimize the failure mechanisms. The most common through-thickness reinforcements include stitching (Fig. 1.11(a)), 3D weaving (Fig. 1.11(b)), z-pinning (Fig. 1.11(c)) and carbon nanotubes (CNTs) (Fig. 1.11(d)). However, these methods have also shown to

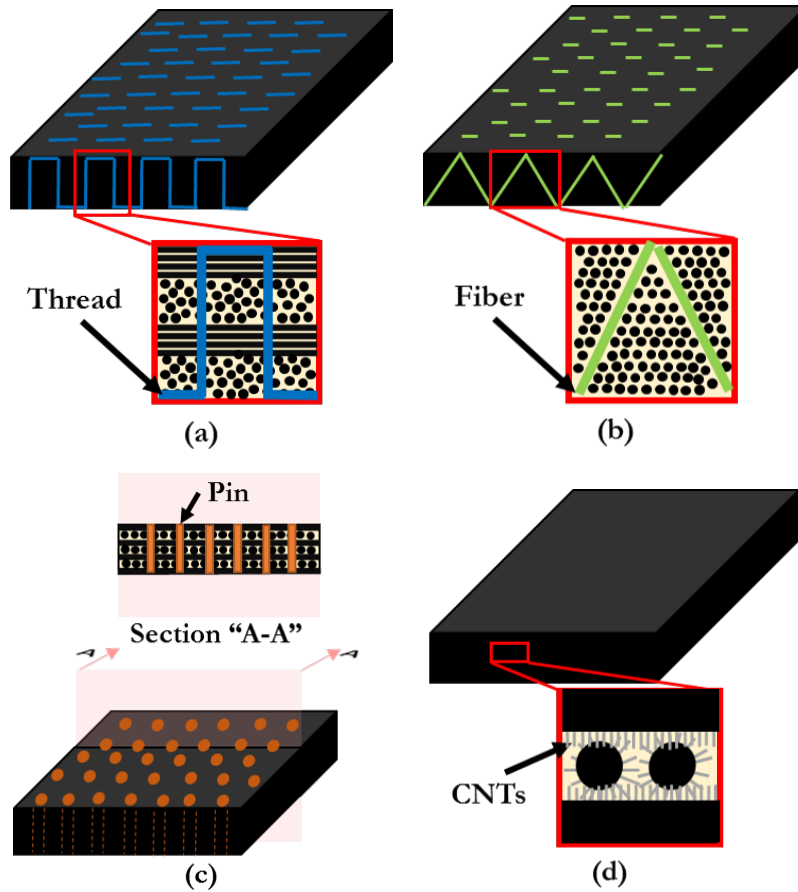


Figure 1.11: Through-thickness reinforcement: (a) stitching; (b) 3D weaving; (c) z-pinning; (d) carbon nanotubes (CNTs)

decrease the in-plane properties of the laminates, which results in lowering the mechanical properties of the FRP composites. For example, z-pinning and stitching tend to break fibers due to the forcible penetration through the layers of fabric [27, 28]. 3D weaving tends to change the fiber volume fraction [27]. The volume fraction is very important because it determines the overall mechanical properties of the FRP composites. CNTs do not distribute uniformly throughout the fabric and are not feasible due to the fact that the layers of fabric are heated up to a temperature of 650 °C [25, 29]. In this thesis, a low-temperature solution-based growth of ZnO nanowires on the surface of the reinforcing fabric is proposed as interlaminar matrix reinforcement.

1.6 Scope and Outline of the Thesis

The use of FRP composites in aerospace, naval and automobiles applications has gained popularity due to their high strength-to-weight ratio and tailorable mechanical properties. However, the interlaminar matrix region is fragile and it can lead to premature failure of the composite. Strengthening this interface improves the composites response to different failure mechanisms, especially for delamination. Damage resistance and durability of woven carbon composites reinforced with nanowires in the interlaminar regions is investigated. First, the response under quasi-static loading (Mode-I and Mode-II) is described in Chapter 2. Followed by the response under dynamic loading (impact) in Chapter 3. The thesis concludes with Chapter 4 by summarizing the main results of this research (Chapter 2 and 3) with a discussion and contributions on future work.

Chapter 2

Nanowire Reinforcement of Woven Composites for Enhancing Interlaminar Fracture Toughness

2.1 Introduction

Composite materials have become an attractive replacement of conventional materials such as steel or aluminum in order to improve the performance and reduce the weight of high performance structures [30]. Their use has been successfully integrated into aerospace vehicles, wind energy turbine blades, rockets, marine structures and automobiles [31] due to their tailorable mechanical properties, high specific stiffness, strength-to-weight ratios, corrosion and fatigue resistance [32, 33]. In particular, sandwich composites are used in ship hulls due to their high bending stiffness. Sandwich composites consist of two facesheets and core sandwiched between them. For improving the damage resistance and durability of sandwich composites, it is essential to improve the properties of facesheet and core. In this paper, the focus is on improving the interlaminar fracture toughness of carbon fiber reinforced facesheet composites. Carbon fiber-reinforced woven composites consist of layers of woven carbon fabric in polymer matrix. Although, the in-plane mechanical properties of these composites are strong and stiff, the resin-rich region between the carbon fiber layers of the composite, which is known as interlaminar region, is susceptible to damage and can result in premature failure of the composite [24, 25]. The life of a composite structure depends on its response to different failure mechanisms, such as delamination or interlaminar fracture, matrix cracking, matrix-fiber debonding, fiber breaking fiber pullout, etc. [34, 35].

Delamination or interlaminar fracture is one of the most common failure mechanisms in composites [34]. Delamination can occur due to manufacturing defects such as bad layup, crack between layers, weaker matrix phase, etc. or in-service due to interlaminar stresses,

impact, static overload and fatigue [36, 37, 38, 39, 27]. This often results in a reduction of stiffness and strength of the composites leading to global failure of the composite structure. Therefore, in this paper, interlaminar fracture toughness is investigated to establish the damage resistance and tolerance of a composite structure. Interlaminar fracture toughness is the amount of energy required to create fracture surfaces under three fracture modes: Mode-I (opening mode), Mode-II (sliding shear mode) and Mode-III (scissoring shear mode) [36, 40]. The focus of this paper is on enhancing the pure Mode-I and Mode-II interlaminar fracture of carbon fiber woven textile composites.

Different through-thickness reinforcements have been studied by earlier researchers, including stitching, weaving, braiding [27], z-pins [28] to improve the interlaminar fracture toughness of composites. Though an increase in through-thickness response was observed, these methods have shown to decrease the in-plane properties due to reduction in the in-plane volume fraction, damaging the reinforcing fibers or by creating large resin pockets [27, 41]. Another method is the use of nanofiber carbon nanotubes (CNTs) on the surface of the dry fabric by chemical vapor deposition. However, CNTs do not distribute uniformly and they tend to create bundles and branches [25, 42]. Further, the techniques that currently exist to disperse the CNTs tend to damage the carbon fiber [25, 43, 29]. Besides, several studies have reported a decrease in the tensile strength of the fibers after CNTs were grown on them [41]. Qian et. al. [44] reported a decrease in the fiber tensile properties by nearly 55%. To prevent damage in the fiber due to high growth temperature and reduction of in-plane properties, a low-temperature solution-based fabrication of ZnO nanowires as interlaminar reinforcements is studied in this paper.

According to Kong et al. [45], different types of nanowires can enhance the interfacial mechanical properties; however, ZnO nanowires are expected to be less prone to impact damage. Recent results from Hwang et al. [46] have shown that vertically aligned ZnO nanowires lead to approximately 23 times higher energy absorption and 11 times higher peak load compared to pristine composites. ZnO nanowires also have piezoelectric and semiconducting properties, which make them well suitable for solar cells [47], dynamic

sensors [48] and energy harvesting materials [49]. A recent study by Lin et al. [50] has shown that ZnO nanowires improve the interfacial shear strength of the individual carbon fibers by 113% and the lamina shear strength and modulus by 37.8% and 38.8%, respectively. In the current paper, the influence of ZnO nanowire on the Mode-I and Mode-II interlaminar fracture toughness of carbon fiber woven composites is investigated. This is the first time ZnO nanowires have been used as means to improve the interlaminar fracture toughness for woven composites.

Carbon fiber woven composites are primarily studied in this paper. ZnO nanowires are synthesized on dry fabric, and the composites are manufactured using Vacuum Assisted Resin Transfer Molding (VARTM) process. The interlaminar Mode-I and Mode-II fracture toughness with and without nanowires are compared using double cantilever beam (DCB) and end notched flexure (ENF) tests, respectively. Significant improvement in Mode-I and Mode-II fracture toughness of the interfaces was observed due to ZnO nanowire reinforcement.

The paper is organized in the following sections: A brief description of the VARTM process for composites manufacturing and ZnO nanowire synthesis on fabric is given in the “Manufacturing” Section, followed by the test methods used to determine Mode-I and Mode-II fracture toughness values in “Interlaminar Fracture Toughness” Section. Finally, a comparison of interlaminar fracture toughness values between laminates with and without ZnO nanowire reinforcement is provided in “Discussion of Results” Section, followed by conclusions.

2.2 Manufacturing

2.2.1 VARTM Process for Composite Manufacturing

VARTM process [51] was used to manufacture the woven composites with and without ZnO nanowires. Laminates were fabricated by placing layers of dry carbon fabric in a mold with flow media, like breather, nylon peel ply, etc. as shown in Fig. 2.1(a). This was followed by enclosing the mold in a vacuum bag (see Fig. 2.1(b)) and drawing it into a vacuum in order

to aid infiltration of the resin [51]. Laminates with 8 layers of dry fabric for Mode-I and

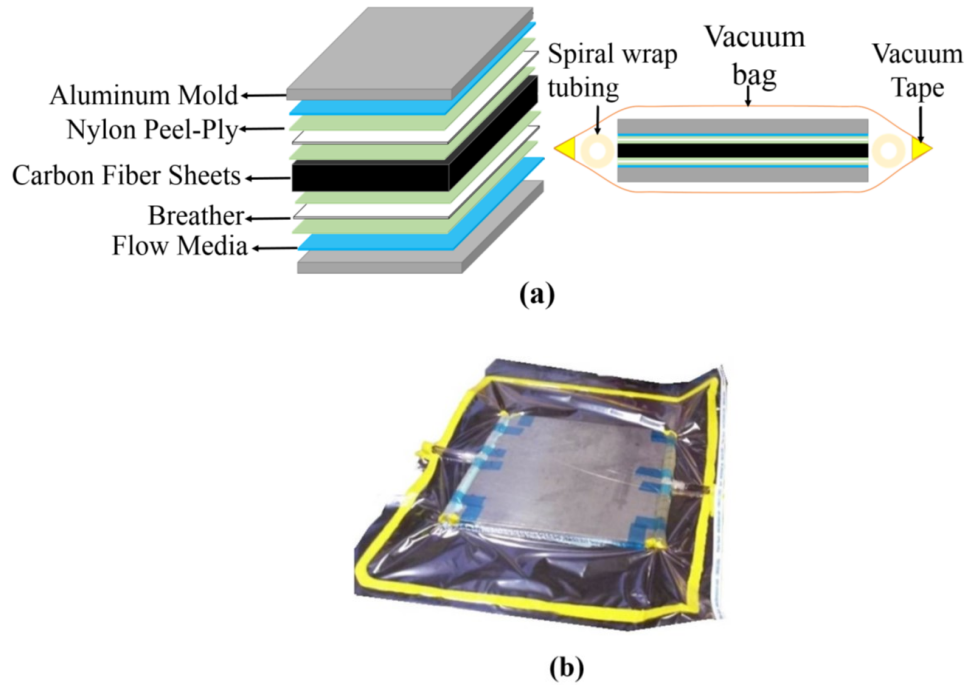


Figure 2.1: (a) VARTM configuration for the 2D carbon woven composite; (b) Laminate preparation in progress using VARTM process

20 layers for Mode-II were manufactured. Dry fabrics of woven (plain weave) were used as reinforcement with Vinyl Ester resin and Methyl Ethyl Ketone Peroxide (MEKP) hardener as matrix material. The resin was catalyzed with 1.25% MEKP (by weight) and mixed thoroughly for one minute as recommended by the manufacturer. All the specimens (with and without ZnO nanowires) for DCB and ENF tests were fabricated as one laminate as shown in Fig. 2.2(a) and Fig. 2.2(b) to ensure that the curing conditions were identical. Teflon sheet of 0.05 mm (0.002 in.) thickness was placed between the 4th and the 5th layers to create a pre-crack for the DCB samples (Fig. 2.2(a)), and between the 10th and 11th layers for the ENF samples (Fig. 2.2(b)). Further, ZnO nanowires were synthesized on the surfaces of the 4th and the 5th layers for Mode-I and on the surfaces of the 10th

and 11th layers for Mode-II, thereby, reinforcing the fracturing interface of the DCB and ENF samples, respectively. Nanowire synthesis on dry fabric is described in the following section.

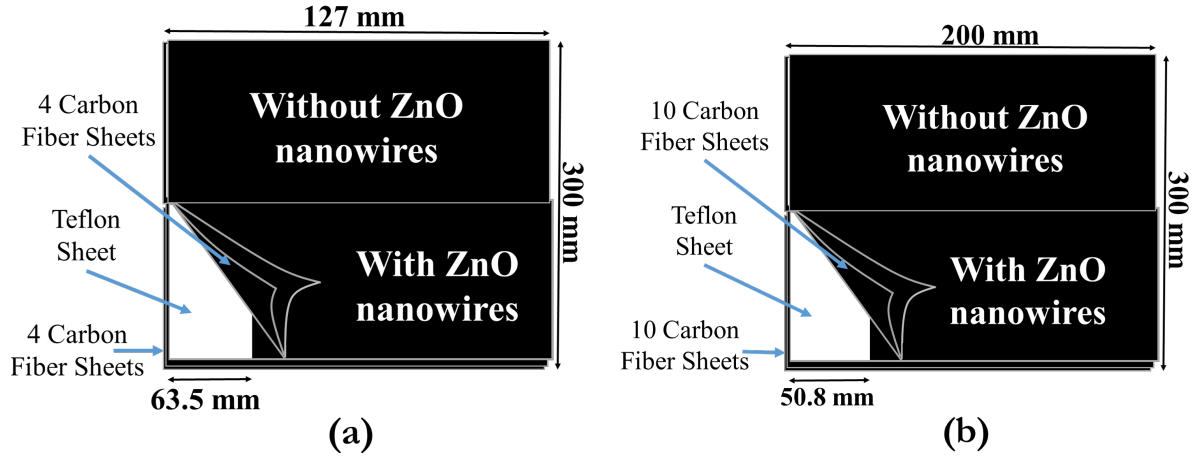


Figure 2.2: (a) Teflon sheet insert to simulate a crack for DCB sample; (b) Teflon sheet insert to simulate a crack for ENF sample

2.2.2 ZnO Nanowire Synthesis on Dry Fabric

ZnO nanowires have very strong interaction with carbon fibers as previous studies have suggested [52]. Functional groups, like hydroxyl, carbonyl, and carboxylic acid, have been found in carbon fibers that create a strong chemical bonding with ZnO [53, 54, 55]. ZnO nanowires added at the mid-plane of the laminate were synthesized using a hydrothermal method, where ZnO nanoparticle seed layer was deposited on a woven carbon fiber surface by dip coating [56]. ZnO nanoparticles were formed by mixing together solutions of zinc acetate dihydrate and ethanol with sodium hydroxide and ethanol at a volume ratio of 18:7 at 55°C [57]. Then, the carbon fibers were covered by ZnO nanoparticles by dip coating [50]. After that, nanowires were grown in a glass beaker on a hot plate, where the deposition on carbon fibers occurred in an aqueous solution of zinc nitrate hydrate and hexamethylenetetramine (HMTA). The temperature of the solution was maintained at 90°C

for 4 hours. Finally, the carbon fiber layers were removed from the solution and were rinsed with 18.2 MΩ water and dried at 100°C [50]. A low-molecular-weight Polyethylenimine (PEI, Aldrich, $M_w = 25,000$) was added to aid uniform growth of nanowires [58]. The morphology (diameter, length, and orientation) and quality of ZnO nanowires synthesized on carbon fibers can be controlled through multiple parameters: temperature, solution concentration, ZnO nanoparticle size, and growth time. The approximate final geometry of the ZnO nanowires in the current study was 50 nm diameter and 500 nm length [50]. Fig. 3.7 shows SEM images of the resulting ZnO nanowires grown on the woven fabric at different scales.

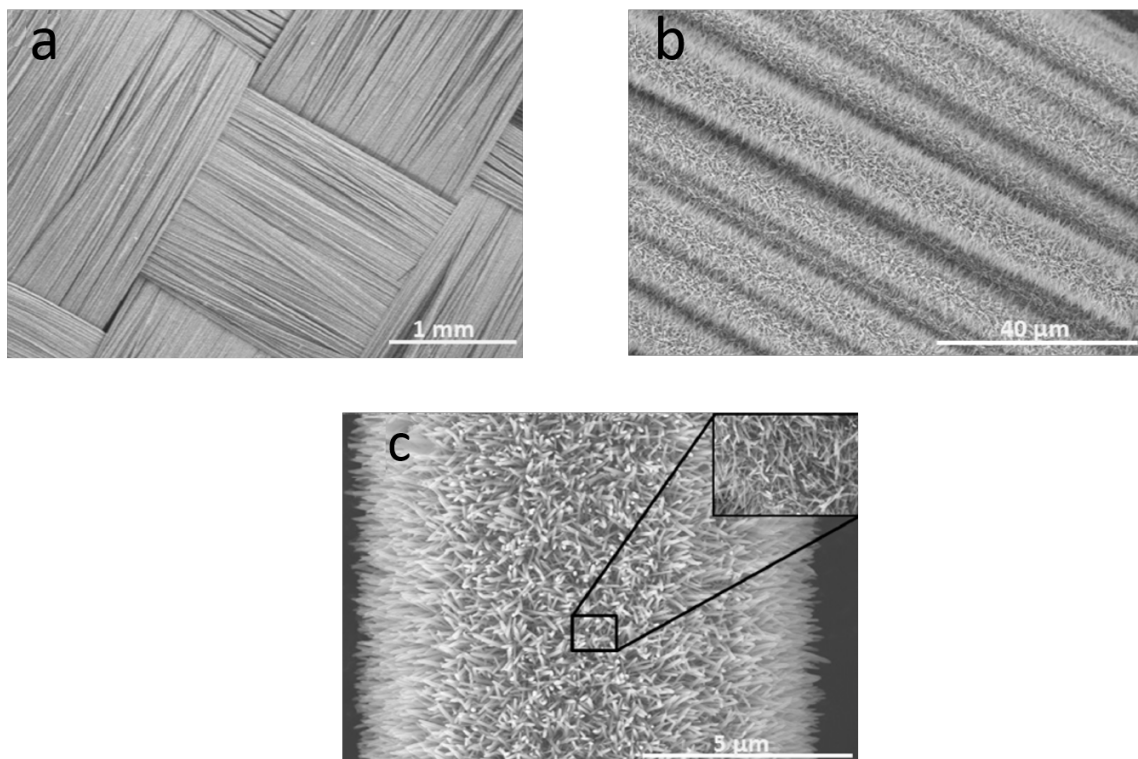


Figure 2.3: ZnO nanowires grown on 2D woven carbon fiber at different scale a) 1 mm, b) 40 μm and c) 5 μm

2.3 Interlaminar Fracture Toughness

Mode-I fracture toughness tests were performed following the double cantilever beam (DCB) test method. Other possible tests are the wedge-insert-fracture (WIF) [35] and compression tension (CT) [34]. Mode-II fracture toughness tests were performed following the end-notched flexure (ENF) test method. According to Wang and Williams [59], the two common test geometries for Mode-II tests are the end-loaded-split (ELS) and the ENF specimens. 3-ENF was originally proposed for testing, which was later developed into the S-ENF, T-ENF and 4-ENF methods [60]. However, according to Morais and Pereira [61], ENF test is the best method for Mode-II due to its simplicity, negligible friction effects and low tendency for geometric non-linearity [62].

2.3.1 Mode-I Fracture Toughness: Double Cantilever Beam (DCB)

Mode-I interlaminar fracture toughness, which is the critical strain energy release in J/m^2 , was determined using DCB test. The DCB specimen typically consists of a rectangular uniform thickness laminated composite with a non-adhesive insert at the mid-plane that serves as a delamination initiator [63]. Opening forces are applied to the DCB specimen using hinges on the top and bottom surfaces at one end of the specimen by controlling the opening displacement, while the load and delamination length are recorded [63].

Test Samples

According to the ASTM Standard D5528-13 [63], the dimensions (Fig. 2.4) of each specimen were 127 mm (5.0 in.) long, 25.4 mm (1.0 in.) wide and 2.54 mm (0.1 in.) thick. A Teflon sheet of 63.5 mm (2.5 in.) length x 25.4 mm (1.0 in.) width x 0.0508 mm (0.002 in.) thickness was inserted to simulate a pre-crack. A pre-crack (about 2 mm) was propagated by loading the hinges with the Instron machine. Eight specimens were tested in total (4 specimens with ZnO nanowires and 4 without ZnO nanowires). The initial delamination length was measured from the point where the load was applied to the end of the pre-crack. Tests were performed on an Instron 8801 with a displacement control unit at a loading rate

of 5 mm/min (recommended loading rate was 1-5 mm/min by ASTM D5528-13). A loading-unloading procedure was followed for crack propagation. That is, the applied displacement was stopped when a significant crack growth accompanied by an abrupt load drop was observed. The crack extension was recorded and the specimens were restored to their original position at an unloading rate of 25 mm/min. About 4-5 loading-unloading cycles were conducted for each DCB specimen. All tests were performed in the Manufacturing and Mechanics Lab, which is a part of the Challenger-Columbia Structures and Materials Lab at the University of Texas at El Paso.

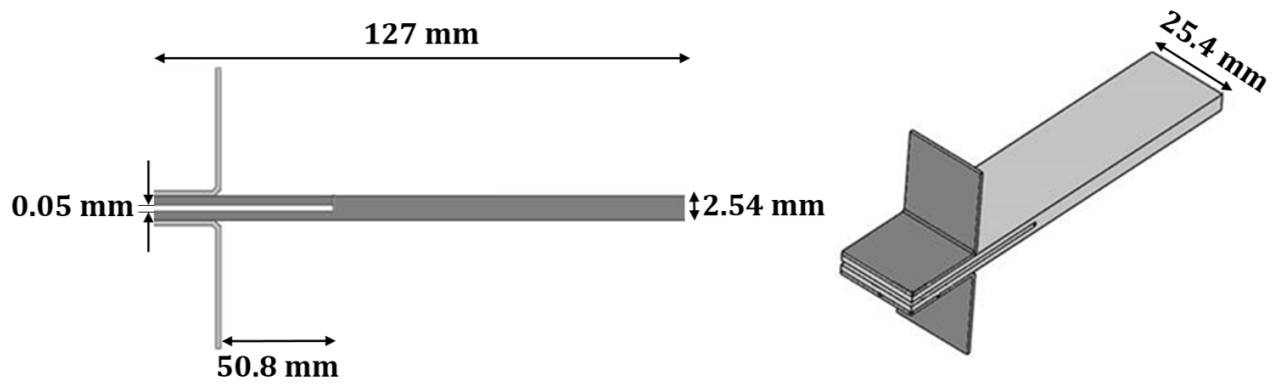


Figure 2.4: Sample dimensions for DCB test

Complex data reduction methods were used to calculate the critical strain energy release rate, G_{IC} , which is influenced by the accuracy of the measured load, displacement, crack length and the change in compliance with crack length. Three data reduction methods were applied to the load-displacement data obtained from the tests: (1) modified beam theory (MBT), (2) compliance calibration (CC) and (3) modified compliance calibration method (MCC) as specified in ASTM D5528-13 [63]. Fig. 2.5 shows the DCB test in progress for one of the specimens.

2.3.2 Mode-II Fracture Toughness: End-Notched Flexure (ENF)

Mode-II interlaminar fracture toughness, which is the critical strain energy release rate in J/m^2 , was calculated using ENF test. The ENF specimen consists of a rectangular,



Figure 2.5: DCB test in progress of a carbon fiber laminate with ZnO nanowires

uniform thickness laminated composite with a non-adhesive insert at the mid-plane that acts as a crack initiator [64]. The ENF specimen is loaded in a three point bend fixture that consists of two support points at the bottom and one load point at the top of the specimen at the mid-span [65]. The load, center point displacement and crack length are measured and recorded during displacement controlled tests.

Test Samples

According to the ASTM Standard D7905/D7905M-14 [64], the dimensions (Fig. 2.6) of each specimen were 200 mm (8.0 in.) long, 25.4 mm (1.0 in.) wide and 3.4 mm (0.1 in.) thick. A Teflon sheet of 50.8 mm (2.5 in.) length x 25.4 mm (1.0 in.) width x 0.05 mm (0.002 in.) thickness was inserted to simulate a pre-crack. Tests were performed on an Instron 8801 at a loading rate of 0.5 mm/min. Eight specimens were tested in total (4 specimens with ZnO nanowires and 4 without ZnO nanowires).

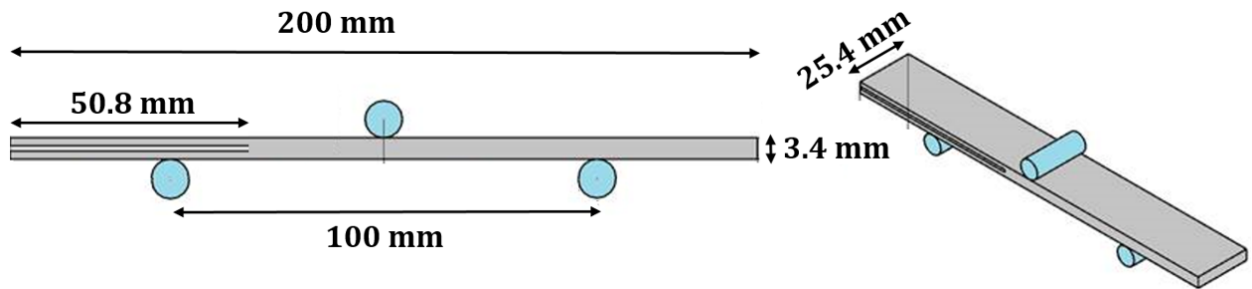


Figure 2.6: Sample dimensions for ENF test

Compliance calibration (CC) method is provided in ASTM D7905 [64] to calculate the

Mode-II interlaminar fracture toughness value. The specimen was positioned in a three point bend fixture when the crack length was equal to 30 mm. The specimen was loaded until the crack propagates and an abrupt drop in force was observed. The unloading rate was 0.5 mm/min. The compliance (C) was determined by linear least squares regression analysis of slope of the load-displacement curve. Then, the fracture toughness was calculated using the CC method as described in ASTM D7905. Fig. 2.7 shows the ENF test in progress for one of the specimens.



Figure 2.7: ENF test in progress of a carbon fiber laminate with ZnO nanowires

2.4 Discussion of Results

Interlaminar Fracture toughness values of composites with and without nanowires were compared to evaluate the influence of ZnO nanowire reinforcement.

2.4.1 Mode-I Fracture Toughness: Double Cantilever Beam (DCB)

Mode-I fracture toughness (G_{IC}) values of composites with and without nanowires were compared. Fig. 2.8 shows the load-displacement response of one specimen without nanowires. As explained before, the specimen was loaded until an abrupt drop in load was observed. The extent of crack propagation was measured, and then the specimen was unloaded to restore to its original position. This process was repeated until the next load drop occurred and the load-displacement plot for 4 cycles for a specimen is shown in Fig. 2.8.

Fig. 2.9 shows the load-displacement curve of one of the specimens with ZnO nanowires. The sample without ZnO nanowires (Fig. 2.8) showed larger drops in load corresponding to crack extension. On the other hand, the load did not drop as drastically in the spec-

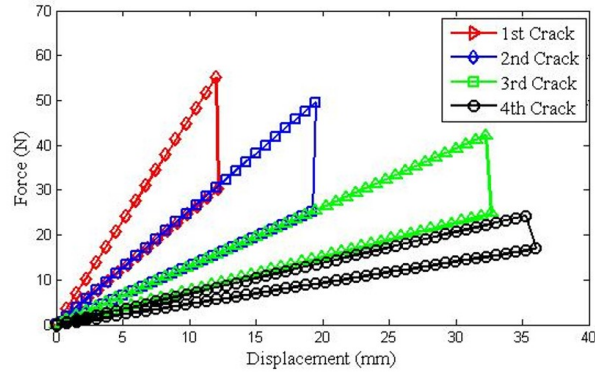


Figure 2.8: Typical load-displacement response of a DCB test specimen without nanowires

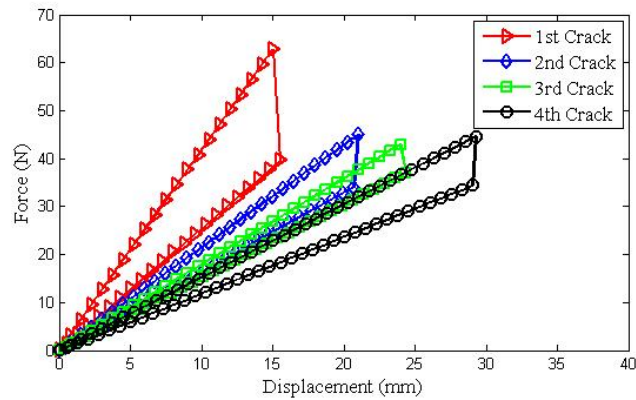


Figure 2.9: Typical load-displacement response of a DCB test specimen with nanowires

imen with ZnO nanowires (Fig. 2.9). As stated before, G_{IC} values were calculated with three reduction methods: MBT, CC and MCC, and the values are shown in Table 2.1 and 2.2 for specimens without and with ZnO nanowires, respectively. ZnO nanowire interlaminar reinforcement showed an increase of approximately 66.5% with MBT method, approximately 84.9% with CC method, approximately 72.6% with MCC method. Therefore, ZnO nanowires appear to greatly improve the Mode-I interlaminar fracture toughness of carbon woven composites. This increase can be attributed to the bridging effect and cohesive matrix failure of the laminate. An analysis of the surface of single fiber showed a cohesive matrix failure, which support resistance of the nanowire towards the formation of

Table 2.1: G_{IC} (kJ/m^2) without ZnO nanowires

Specimen	MBT	CC	MCC
1	0.442	0.414	0.465
2	0.424	0.427	0.477
3	0.424	0.376	0.418
4	0.454	0.505	0.434
Average	0.430 ± 0.001	0.431 ± 0.047	0.449 ± 0.023

Table 2.2: G_{IC} (kJ/m^2) with ZnO nanowires

Specimen	MBT	CC	MCC
1	0.747	0.772	0.726
2	0.683	0.777	0.734
3	0.718	0.726	0.809
4	0.760	0.914	0.832
Average	0.716 ± 0.026	0.797 ± 0.070	0.775 ± 0.056

new surfaces at the interlaminar regions[50].

2.4.2 Mode-II Fracture Toughness: End-Notched Flexure (ENF)

Fig. 2.10 and Fig. 2.11 show the load-displacement response of specimens without and with ZnO nanowire reinforcement for ENF tests. The displacements are normalized by the displacement corresponding to the peak load to account for the slight increase in thickness due to nanowire reinforcement.

During the experiments, it was noticed that the crack progression in the sample without ZnO nanowires was more sudden as compared to the samples with ZnO nanowires. This is manifested by steeper drop in the post peak response of the samples without ZnO nanowires (Fig. 2.10) as compared to the gradual drop in peak load for samples with ZnO nanowires (Fig. 2.11).

As stated before, G_{IIC} values were calculated using the CC reduction method. G_{IIC} values calculated for the specimens without and with ZnO nanowires are given in Table 2.3.

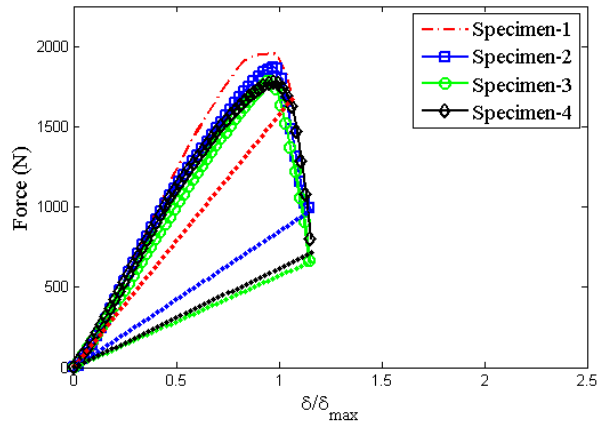


Figure 2.10: Load-displacement response for specimens without nanowires for ENF

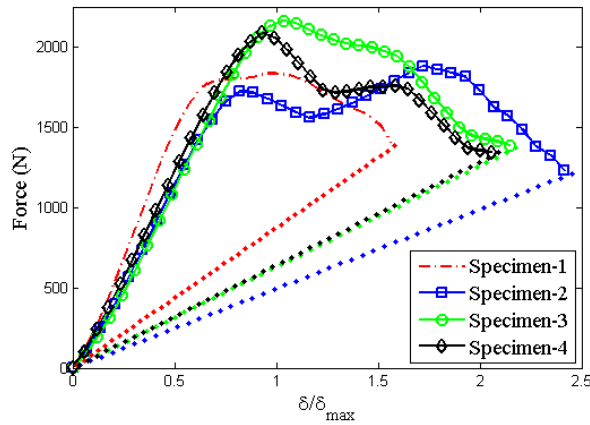


Figure 2.11: Load-displacement response for specimens with nanowires

ZnO nanowire reinforcement showed an average increase of approximately 28% with CC method. This increase is attributed to the shearing effect of ZnO nanowires at the laminate interfaces, thus, reducing the ease of creating new smooth fracture surfaces. Therefore, ZnO nanowires appear to improve the Mode-II interlaminar fracture toughness of carbon woven composites.

Table 2.3: G_{IIC} (kJ/m^2)

Specimen	without ZnO	with ZnO
1	0.422	0.584
2	0.459	0.557
3	0.426	0.513
4	0.437	0.571
Average	0.436 ± 0.014	0.556 ± 0.027

2.4.3 Fractographic Analysis

The fractured surfaces were examined under a scanning electron microscope (SEM) in order to explore the interlaminar fracture mechanism of the specimens with and without ZnO nanowires. Fracture surfaces in both cases were restricted in the mid-plane interlaminar region of the composite. In samples without ZnO nanowires, the crack propagated predominantly through the resin as observed in Fig. 2.12(b). That is, the interface is smooth with only a small amount of fiber separation at the interface. Whereas, for samples with ZnO nanowires, a large amount of fiber separation at the interface was observed as shown in Fig. 2.12(a), which is attributed to the ZnO nanowires at the interfaces. Based on the observations, it is hypothesized that the ZnO nanowires improve the bonding between the interfaces. Due to enhanced shear resistance imparted by the ZnO nanowires, the fracture surface progression is accompanied by fiber separation from the layers, which appears to improve the Mode-II interlaminar fracture toughness. That is, a higher resistance is present in the sample with ZnO nanowires, where the fracture surface not only propagates through the interlaminar region, but also pulls the carbon fibers, as seen in Fig. 2.12(c) and Fig. 2.12(d).

2.5 Conclusion

In this paper, Mode-I and Mode-II interlaminar fracture toughness values of carbon fiber woven composite facesheets with and without ZnO nanowire reinforcement at the interlam-

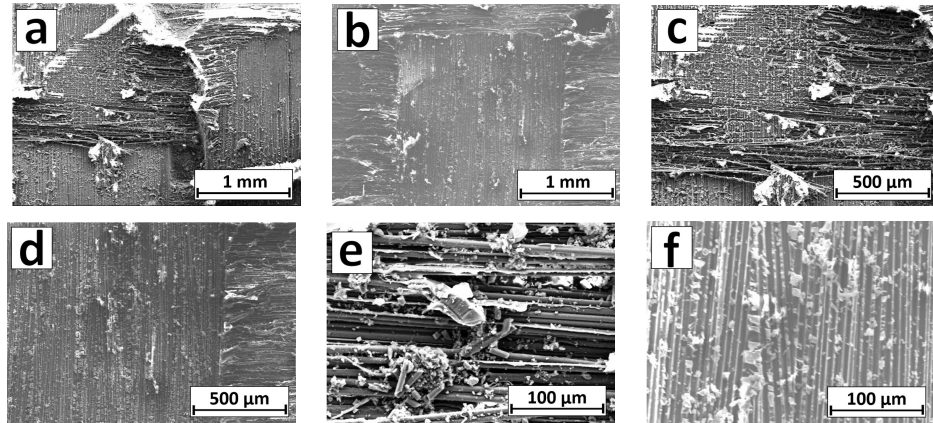


Figure 2.12: (a) Fracture surface for a specimen with ZnO nanowires (Scale: 1 mm); (b) Fracture surface for a specimen without ZnO nanowires (Scale: 1 mm); (c) Fracture surface for a specimen with ZnO nanowires (Scale: 500 μm); (d) Fracture surface for a specimen without ZnO nanowires (Scale: 500 μm); (e) Fracture surface for a specimen with ZnO nanowires (Scale: 100 μm); (f) Fracture surface for a specimen with ZnO nanowires (Scale: 100 μm)

inar regions were compared. Double cantilever beam (DCB) tests were used to determine the Mode-I fracture toughness values with three data reduction methods: modified beam theory (MBT), compliance calibration (CC) and modified compliance calibration (MCC). End-notched flexure (ENF) tests were used to determine the Mode-II fracture toughness values by compliance calibration (CC) method. Eight specimens were tested for each mode, four with ZnO nanowires and four without. This study revealed that the Mode-I interlaminar fracture toughness increased significantly: approximately 66.5% from MBT, 84.9% from CC method and 72.6% MCC method. For Mode-II, the interlaminar fracture toughness increased by approximately 28% in comparison to the samples without ZnO nanowires. Therefore, this study showed very promising results by adding ZnO nanowires at the interlaminar regions to improve their Mode-I and Mode-II fracture toughness values.

Chapter 3

Interlaminar Reinforcement for Enhancing Low-Velocity Impact Response of Woven Composites

3.1 Introduction

Sandwich composites are widely use in ship hulls due to their high bending stiffness to weight ratio, which typically consist of a core sandwiched between two face sheets. A major drawback of sandwich composites is their low resistance to dynamic impact loading. Hence, it is essential to improve the properties of the face sheets, the core and the adhesion between them for improving the damage resistance and durability of sandwich composites. In this paper, the focus is on improving the impact response of woven carbon fiber reinforced face sheet composites.

Carbon fiber reinforced woven composites consist of layers of woven carbon fabric reinforced in a polymer matrix. The region between the layers of the reinforcing fabric is a resin-rich region known as the “interlaminar region”, which are highly susceptible to damage that could lead to premature failure of the composite [24, 25]. Specially, loads like face impact or edgewise compression can cause significant damage in the interlaminar regions. Often, the residual strength of composites is drastically reduced by impact damage in the transverse direction due to the lack of reinforcement in the interlaminar regions.

Low-velocity impact, like tool drop during manufacturing or repair [66, 67] can cause significant damage in the interior of these composites. Dynamic impact is generally divided into low or high velocity impact [68, 69]. Typical low-velocity impact occurs at a velocity below 10 m/s [70]. Common failure modes observed during low-velocity impact are fiber breakage, matrix cracking and delamination [66, 67, 71, 72, 73]. Of these, delamination is one of the most common failure mechanisms [34] observed during low-velocity impact [74], which often results in the reduction of stiffness, strength, durability and stability of the

composite resulting in the global failure of the structure [75, 76].

Several through-thickness reinforcements have been investigated by earlier researchers to improve the impact resistance of composites. Sohn and Hu [77] used chopped Kevlar fibers as through-thickness reinforcement in unidirectional composites in the out-plane direction of the fibers. Although, a 100% increase in the values of interlaminar fracture toughness was observed, the compressive strength appeared to reduce up to 15%. Other methods such as z-pinning and stitching have shown to decrease the area of damage and increase the compression after impact (CAI) response. However, these methods appear to decrease the in-plane properties of the laminate due to undesired effects like fiber breakage and creation of large resin pockets around a z-pin or thread [27, 41]. Carbon nanotubes (CNTs) have also been proposed as potential through-thickness reinforcements. However, CNTs do not distribute uniformly throughout the fabric. Also, a decrease in the in-plane properties by nearly 55% [44] was reported due to damaged fibers, which is attributed to the high temperature (650 °C) required for the synthesis of CNTs on the fibers [25]. Therefore, a low-temperature solution-based fabrication of Zinc Oxide (ZnO) nanowires as interlaminar reinforcement is explored in this paper to avoid/reduce any such in-plane damage, while improving the through-thickness properties.

Previous researchers [45, 50] have verified that ZnO nanowires have a strong chemical bonding to carbon fibers. Composites with ZnO nanowires have 23 times higher impact energy absorption compared to pristine composites [46]. Also, ZnO nanowires have piezoelectric and semiconducting properties, which make them suitable for solar cells [47], dynamic sensors [48] and energy-harvesting applications [49]. A recent study by Castellanos et al. [78] has shown that ZnO nanowires improve mode I (opening) interlaminar fracture toughness by approximately 74% and mode II (shear) interlaminar fracture toughness by approximately 28% for plain weave carbon composites.

Carbon fiber woven composites are primarily studied in this paper. ZnO nanowires are synthesized on dry fabric and the composites are manufactured using the Vacuum Assisted Resin Transfer Molding (VARTM) process. The impact response and degree of damage of

the laminates with and without ZnO nanowires are then compared to draw conclusions on the influence of interlaminar reinforcement. The paper is organized in the following sections: “Impact Modeling” section describes the modeling approach for determining critical interfaces during impact loading. A brief description of the VARTM process for composite manufacturing and ZnO nanowire synthesis on fabric is given in the “Manufacturing” section. “Experimental Work” section describes the experiments conducted. Finally, a comparison of the degree of damage is provided in the “Results and Discussion” section, followed by conclusions.

3.2 Impact Modeling

A 16-layer laminate was modeled within the finite element method (FEM) framework using a commercially available software (ABAQUS) to determine the interlaminar regions that were more susceptible to impact damage. The laminate model consisted of 31 layers in total: 16 layers of effective plain woven carbon fabric reinforcement and 15 layers of matrix material as shown in Fig. 3.1.

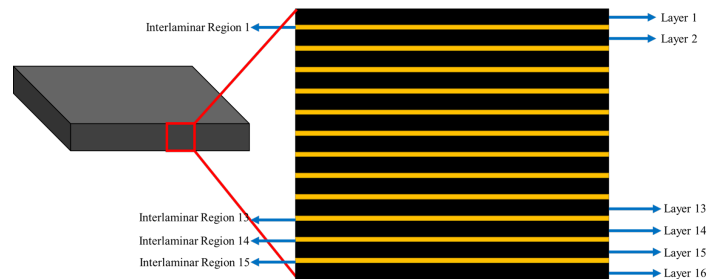


Figure 3.1: Schematic of fabric layers and interlaminar regions of the laminate

The mechanical properties [1] of a plain weave carbon lamina used for the simulations reported in this paper are shown in Table 3.1. The mechanical properties of the interlaminar matrix region assumed to be isotropic were $E_m = 2.5$ GPa and $\nu = 0.3$. A cross-section of the laminate manufactured was examined under a scanning electron microscope (SEM) to obtain an average thickness of the effective woven carbon fabric layers and interlaminar

Table 3.1: Plain weave carbon lamina material constants [1]

E_{11}	E_{22}	E_{33}	ν_{12}	ν_{13}	ν_{23}	G_{12}	G_{13}	G_{23}
(GPa)	(GPa)	(GPa)	(-)	(-)	(-)	(GPa)	(GPa)	(GPa)
48.02	48.02	1.94	0.2	0.48	0.27	0.94	0.77	0.77

matrix regions. The striker was modeled as a rigid body and its motion was governed by a reference point. A circular partition with an area of $\approx 7.0in^2$ ($45.6 cm^2$) (refer to Fig. 3.2(a)) was created on the top and bottom faces of the laminate to simulate the circular aperture of the clamp. All the nodes of the bottom and top clamp were fixed in all the three degrees of freedom. Eight-node 3D reduced elements (C3D8R) were used to mesh the striker and the entire laminate with finer mesh in the center circular region as shown in Fig. 3.2(b). Surface-to-surface contact between the striker and the impacted laminate surface was added by the contact algorithm within the Explicit module of ABAQUS.

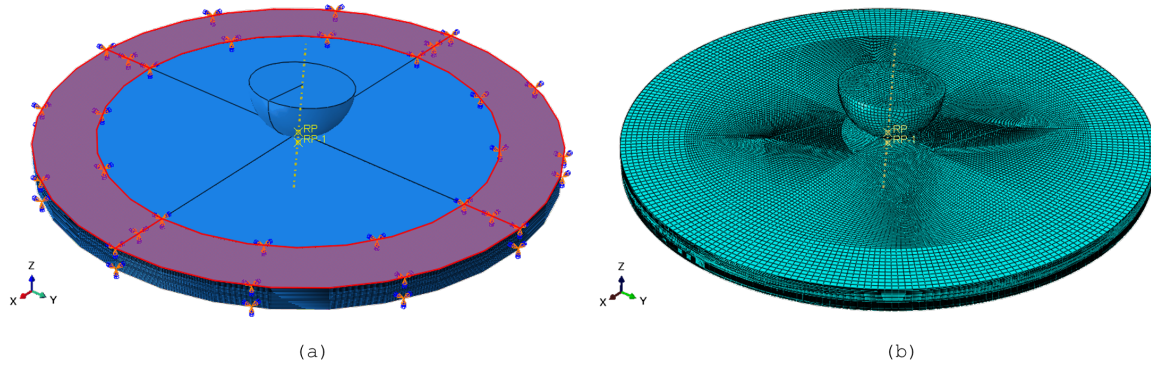


Figure 3.2: (a) Impact model of specimen with boundary conditions; (b) Meshed elements using C3D8R elements

The stresses in the matrix regions were determined at the peak impact force in order to find the interlaminar regions that were more prone to damage. A plot of the contact force-time of the striker was obtained to find the time corresponding to the maximum force applied on the laminate. Point A from Fig. 3.3 corresponds to the simulation start time.

The striker was exactly positioned at the top of the laminate. Point B shows striker hit on the laminate. Point C corresponds to a time between the initial strike and the peak contact force. Point D shows the maximum force imparted to the laminar, in which the striker starts to recede from the surface and rebounds back to its original position. The

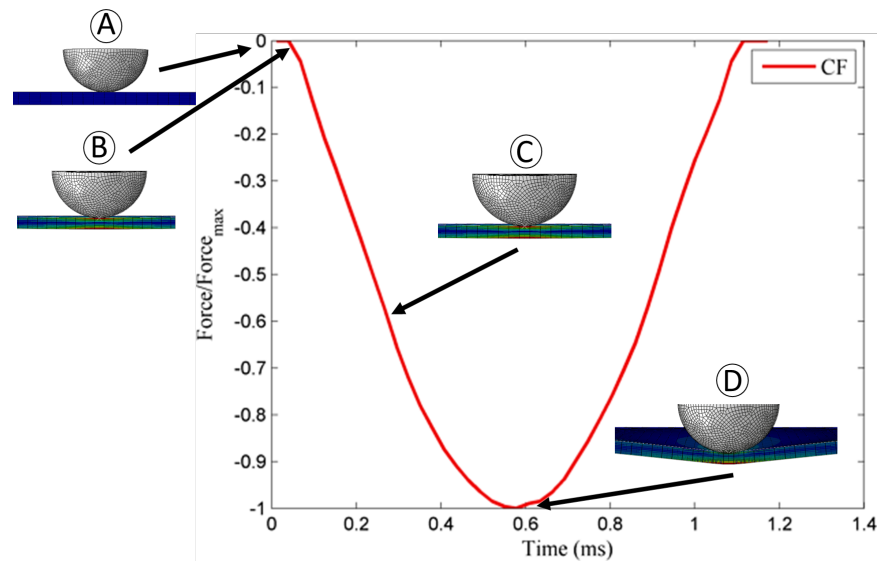


Figure 3.3: Contact force versus time of the impact model

center element in the plane of each interlaminar region was chosen to plot the von Mises stress-time response. Fig. 3.4 shows the plot of the normalized von Mises stress-time of the interlaminar region that experienced higher stresses compared to the others. It was observed that Interlaminar Region-1 (underneath the top impacted layer) and Interlaminar Regions 13, 14 and 15 (3 interlaminar regions towards the bottom layers of the laminate) experienced relatively higher stresses than other interlaminar regions. Hence, ZnO nanowire interlaminar reinforcements were only added to the layers that exhibited at least 50% of the maximum interlaminar stresses obtained from the simulation.

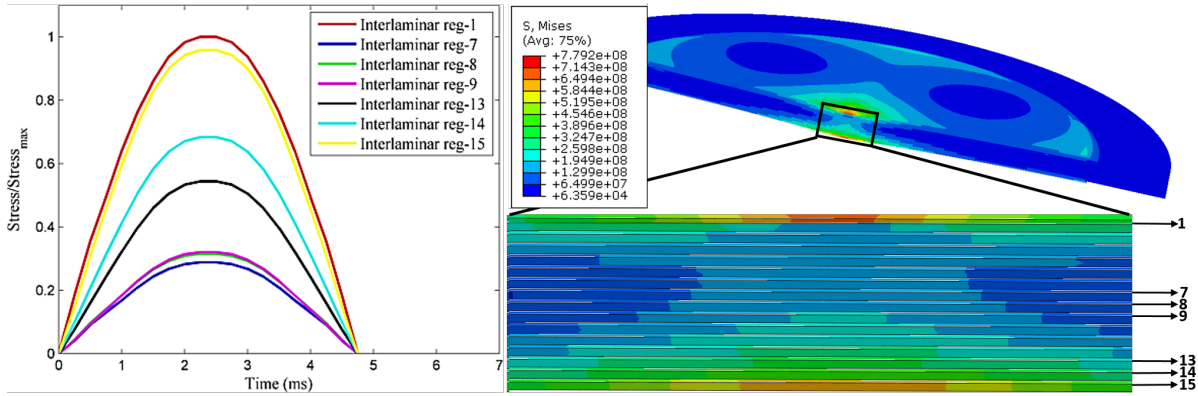


Figure 3.4: Interlaminar regions that exhibit higher stresses

3.3 Manufacturing

3.3.1 VARTM Process for Composite Manufacturing

Woven composites with and without ZnO nanowires were manufactured by VARTM process [51]. Laminates were fabricated by placing layers of dry carbon fabric in an aluminum mold with layers of flow media, breather, nylon peel ply, etc. as shown in Fig. 3.5(a). This was followed by enclosing the mold in a vacuum bag (see Fig. 3.5(b)) and drawing it into vacuum in order to aid the infiltration of resin [51]. Laminates with 16 layers of dry fabric were manufactured according to the ASTM Standard D7136/D7136M. Dry fabrics of woven (plain weave) were used as reinforcement with a mixture of vinyl ester resin and Methyl Ethyl Ketone Peroxide (MEKP) hardener as matrix material. The resin was catalyzed with 1.25% MEKP (by weight) and mixed thoroughly for one minute as recommended by the manufacturer.

Samples with and without ZnO nanowires were manufactured together as shown in Fig. 3.6 to ensure that the curing conditions were identical. A total of 5 laminates of 12 in. (305 mm) by 12 in. (305 mm) were manufactured. 6 samples were obtained (3 samples with ZnO nanowires and 3 without) from each laminate. ZnO nanowires were synthesized on dry fabric at weak interlaminar regions suggested by the simulation of the impact test. From

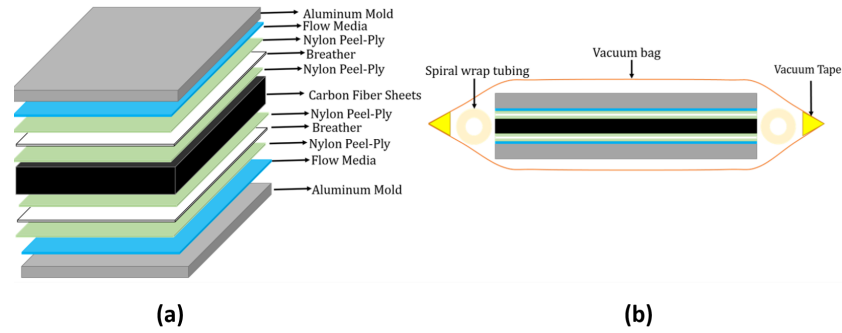


Figure 3.5: VARTM configuration for the carbon woven composite

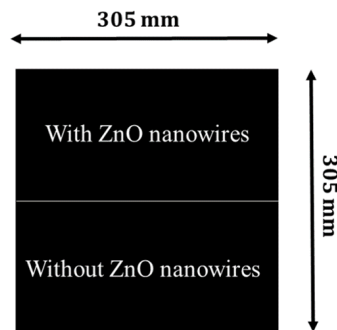


Figure 3.6: Schematic of a 12 in. by 12 in. laminate manufactured

the simulation, the interlaminar regions with the highest stresses were deemed susceptible to delamination. More details about the simulation can be found in “Impact Modeling” section of this paper. Synthesis of nanowires on dry fabric is described in the following section.

3.3.2 ZnO Nanowire Synthesis on Dry Fabric

ZnO nanowires have very strong interaction with carbon fibers as previous studies have suggested [52]. Functional groups, like hydroxyl, carbonyl, and carboxylic acid, have been found in carbon fibers that create a strong chemical bonding with ZnO [53, 54, 55]. The ZnO nanowires added at the mid-plane of the laminate were grown using a hydrothermal method, where ZnO nanoparticle seed layer was deposited on the woven carbon fiber surface by dip

coating [56]. ZnO nanoparticles were formed by a mixing together solutions of zinc acetate dihydrate and ethanol with sodium hydroxide and ethanol at a volume ratio 18:7 at 55°C [57]. Then, the carbon fibers were covered by ZnO nanoparticles by dip coating [50]. After that, nanowires were grown in a glass beaker on a hot plate, where the deposition on carbon fibers occurred in an aqueous solution of zinc nitrate hydrate and hexamethylenetetramine (HMTA). The solution temperature was maintained at 90°C for 4 hours. Finally, the carbon fiber layers were removed from the solution and were rinsed with 18.2 MΩ water and dried at 100°C [50]. A low-molecular-weight Polyethylenimine (PEI, Aldrich, $M_w = 25,000$) was added to aid uniform growth of nanowires [58].

The morphology (diameter, length, and orientation) and quality of ZnO nanowires synthesized on carbon fibers can be controlled through multiple parameters: temperature, solution concentration, ZnO nanoparticle size, and growth time. The approximate final geometry of the ZnO nanowires in the current study was 50 nm diameter and 500 nm length [50]. Fig. 3.7 shows SEM images of the resulting ZnO nanowires grown on the woven fabric at different scales.

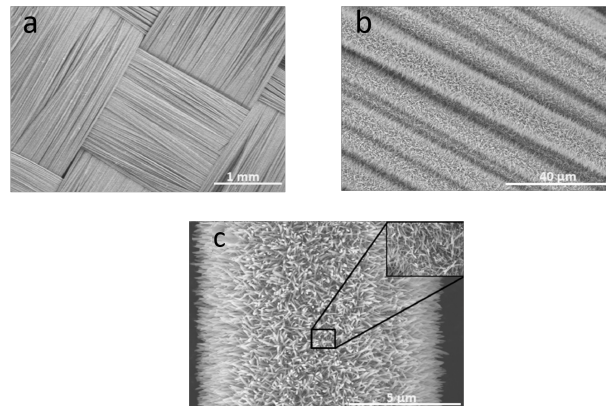


Figure 3.7: ZnO nanowires grown on 2D woven carbon fiber at different scale: a) 1 mm, b) 40 μm and c) 5 μm

3.4 Impact Tests

Drop-weight impact tests were performed using a CEAST 9340 Drop Tower Impact System on rectangular laminate specimens of 4.0 in. (100 mm) long x 4.0 in. (100 mm) wide (refer to Fig. 3.8) and thicknesses 4.49 ± 0.08 mm.

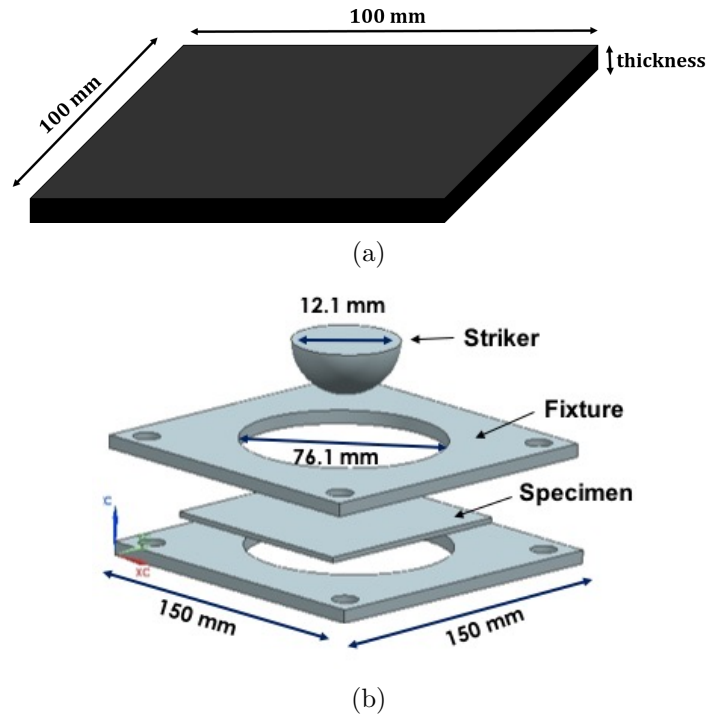


Figure 3.8: (a) Specimen dimensions; (b) Impact fixture schematic

The laminates were clamped between two metal fixtures with a test area of 7.07 in^2 (45.6 cm^2). The impact load using a hemispherical impactor (striker) with a mass of 3.01 kg and a diameter of 0.5 in. (12.7 mm) was concentrated at the center of the specimen in the out-of-plane direction [79] with energies of 2, 5, 10, 20 and 25 Joules for both types of samples (with and without ZnO nanowires). Force-time, energy-time and force-displacement plots were obtained from all the tests.

3.5 Results and Discussion

Impact responses were evaluated in terms of visual damage of the impacted specimens and by calculating the degree of damage. Fig. 3.9 shows the force-time responses from the impact tests normalized by the thickness of each sample with and without ZnO nanowires. Table 3.2 shows the peak force obtained for each test performed. It was observed that the samples with ZnO nanowires have higher peak force than the samples without ZnO, except for the 2 J and 25 J tests. The sample that was impacted with 25 J without ZnO nanowires exhibited more damage and deflection than the sample with ZnO nanowires.

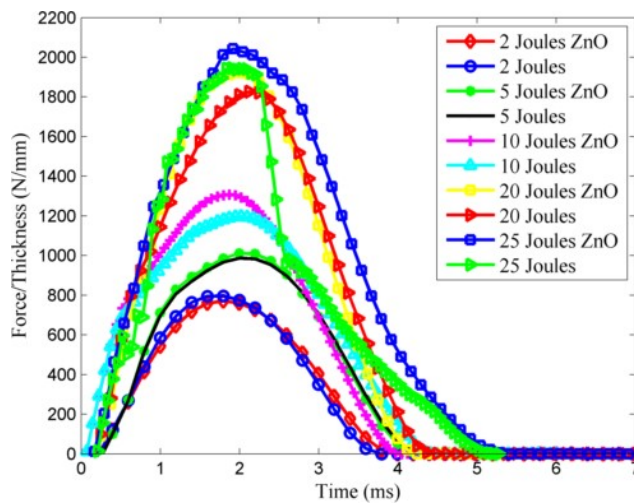


Figure 3.9: Normalized force-time response for energies of 2, 5, 10, 20 and 25J

Table 3.2: Peak force, maximum deflection for samples with and without ZnO nanowires

Energy (J)	Peak Force (N) w/ ZnO	Peak Force (N) w/o ZnO	Max. Deflection (mm) w/ ZnO	Max. Deflection (mm) w/o ZnO
2 J	3564.8	3686.9	1.06	1.09
5 J	4690.9	4526.5	1.69	1.78
10 J	6195.2	5498.1	2.72	2.88
20 J	8848.8	8343.9	3.93	4.05
25 J	9459.3	8871.4	3.54	4.19

Fig. 3.10(a) shows the energy-time responses from the 30 (3 specimens for each tested

energy) specimens that were tested. According to Belingardi and Vadori [80], the degree of damage (D) was defined as the ratio of the absorbed energy to the impact energy (refer to Fig. 3.10(b)). Table 3.3 shows the calculated damage parameter for each specimen.

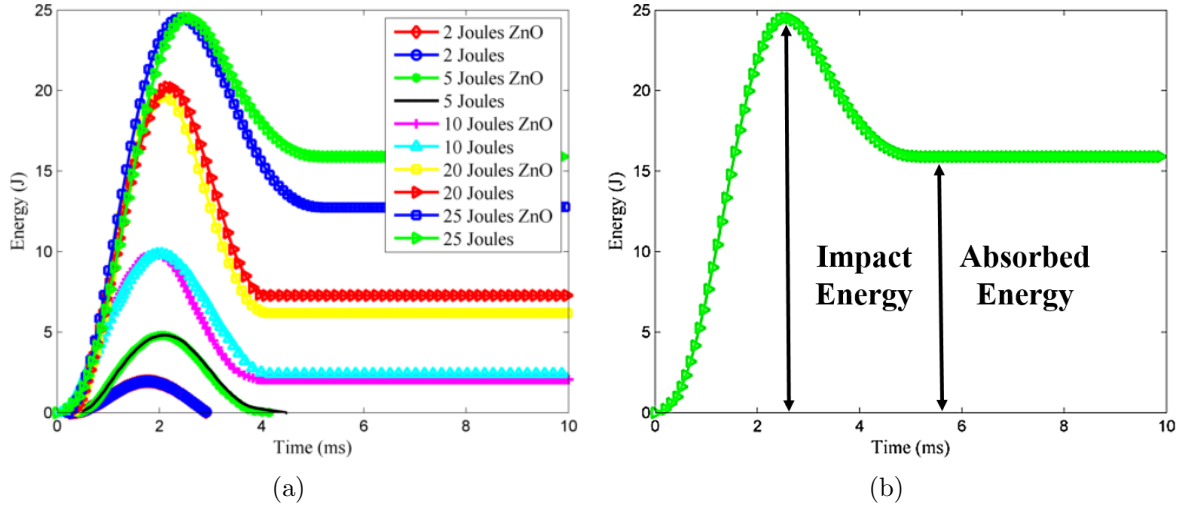


Figure 3.10: (a) Energy vs time graph; (b) Definition of degree of damage

Table 3.3: Degree of damage

Energy J	Damage Degree Sample with ZnO	Damage Degree Sample without ZnO	Percentage Change of the Damage Degree
2 J	0	0	0
5 J	0	0	0
10 J	0.21	0.24	15
20 J	0.31	0.34	9.7
25 J	0.53	0.61	15

It should be noted that the degree of damage was negligible or zero for the specimens impacted with 2 J and 5 J energies, which implies that there was no damage imparted to those laminates and the striker rebounded from the impacted surface. For higher impact energies, the samples with ZnO nanowires manifested lower values of D than the samples without ZnO nanowires, with up to 15% reduction. Hence, ZnO nanowire reinforcement showed an increase in damage resistance for low-velocity impact loading.

Images of the impacted laminates were obtained for the samples with and without ZnO nanowires to visually evaluate the pattern and extent of damage. At low energies (2 J and 5 J), the striker rebounded and no damage was observed in the laminate. For 10 J and 20 J, the damage imparted to the laminate was internal and was not visible to the naked eye. The samples impacted at 10 J with (Fig. 3.11(a)) and without (Fig. 3.11(b)) ZnO nanowires were cut at the middle to examine under scanning electron microscope (SEM). The sample without ZnO nanowires exhibited delamination at the top layer which the sample with ZnO nanowires did not exhibit any damage at the top layer. For the samples impacted with 25

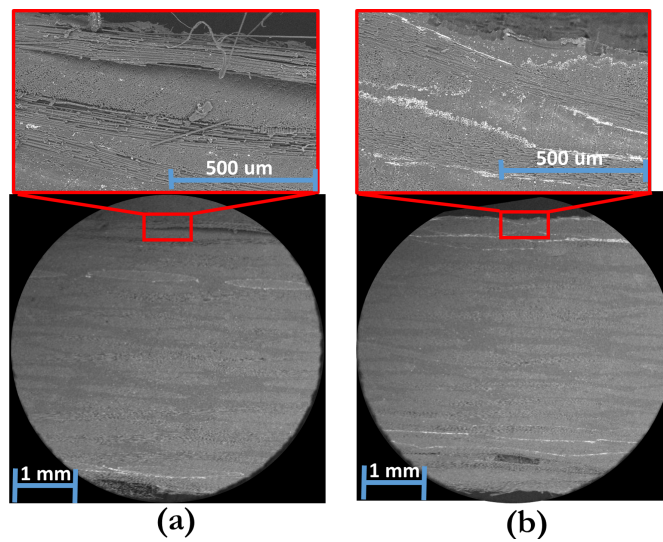


Figure 3.11: Images of the cross-section of the laminate impacted at 10J. (a) Laminate without ZnO nanowires; (b) Laminate with ZnO nanowires.

J energy, a combination of fiber breaking, matrix cracking and delamination damage modes were observed. From Fig. 3.12, it is evident that the top impacted surface of the laminate without ZnO nanowires exhibited larger damage area than the sample with ZnO nanowires. From the bottom surface, the sample without ZnO nanowire exhibited a long radial crack with fiber breakage, while the sample with ZnO nanowire only exhibited matrix crack and there was no fiber breakage. From the cross-sectional view at the center of the laminate, it

was observed that the top layer and bottom layer were separated from the laminate without ZnO nanowires. The sample with ZnO nanowires also exhibited delamination, but it was not as pronounced as the sample without reinforcement. In both cases fiber breakage was seen at the bottom of the laminate.

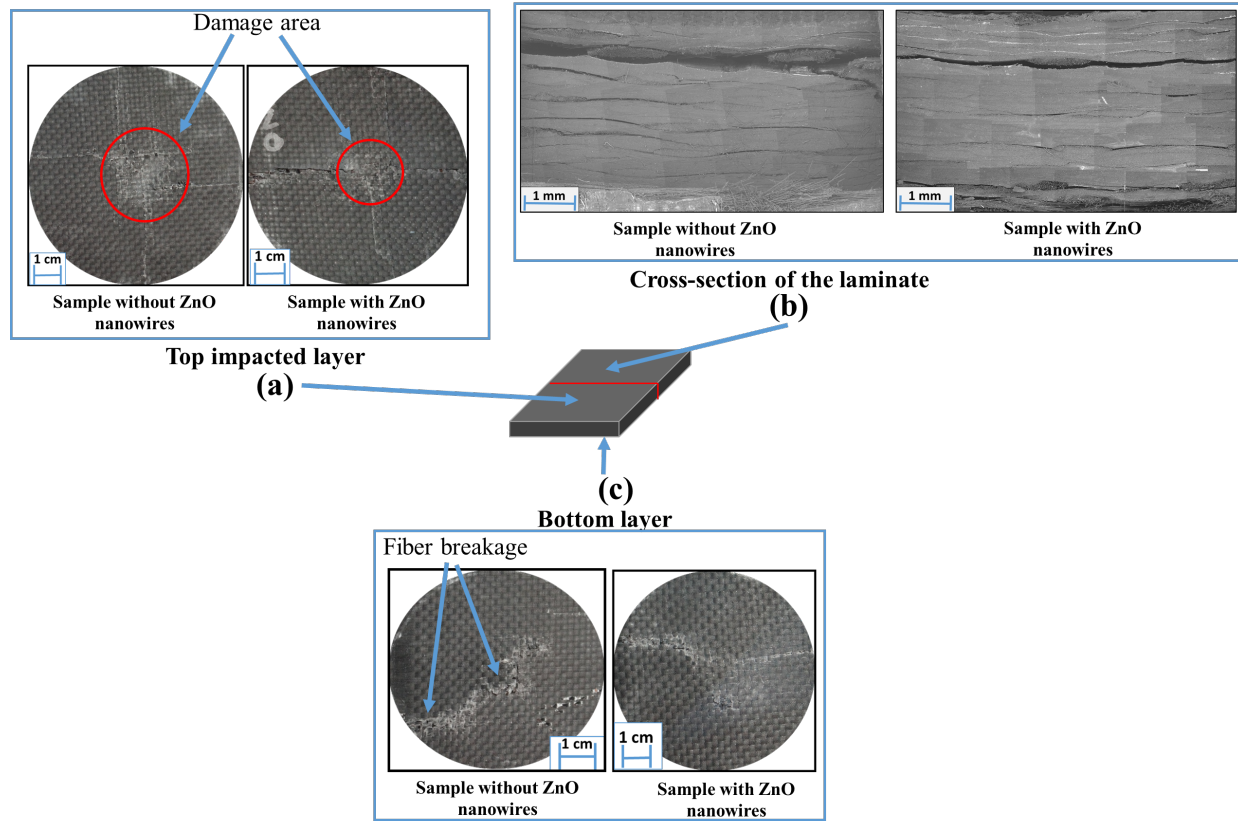


Figure 3.12: Images of top impacted layer, bottom layer and cross-section of the specimens with and without ZnO nanowires impacted at 25 J.

3.6 Conclusion

In this paper, low-velocity impact responses of woven composites with and without ZnO nanowire interlaminar reinforcements were investigated. Interlaminar regions most susceptible to damage were determined by simulating the impact test within the finite element

framework. Through-thickness reinforcements were synthesized along the chosen interfaces and the degree of damage for specimens with and without ZnO nanowires were experimentally determined. The tests revealed that the samples without ZnO nanowires experienced a higher degree of damage in comparison to the samples with ZnO nanowires. Therefore, the study presented in this paper shows the potential of using ZnO nanowires as through-thickness reinforcements in the interlaminar regions of woven composites for improving their impact damage resistance.

Chapter 4

Conclusion and Future Work

4.1 Conclusion

This thesis addresses a new technique to increase the damage tolerance and durability of woven carbon composites. This technique is a through-thickness reinforcement, in which ZnO nanowires are synthesized radially and rigidly along the carbon fibers into the matrix. ZnO nanowires were chosen due to the strong chemical bonding that exist between carbon and ZnO. The Mode-I and Mode-II interlaminar fracture toughness was evaluated for specimens with and without ZnO nanowires. For the reinforced specimens, an increase in the interlaminar fracture toughness was calculated at 74% and 28% for Mode-I and Mode-II, respectively. For dynamic loading, impact responses were evaluated in terms of visual damage and by calculating the degree of damage. It was found that the degree of damage was reduced by approximately 18% when ZnO nanowires were added.

4.2 Major contributions

In this thesis, a low-temperature solution-based growth of ZnO nanowires on the surface of the reinforcing fabric is proposed as interlaminar matrix reinforcement. This new method has proved not to decrease the in-plane properties of the laminate. This is in contrast with current methods, which have shown to decrease the in-plane properties of by to 55%. From the present study, the work on nanowire reinforcement of woven for enhancing interlaminar fracture toughness (Chapter 2) has been accepted for publication in the Journal of Sandwich Structures and Materials. Interlaminar reinforcement for enhancing low-velocity impact response of woven composites (Chapter 3) is being prepared for publication.

4.3 Future work

The study presented demonstrates the potential of using ZnO nanowires as through-thickness reinforcement in the interlaminar regions of woven composites for improving the interlaminar fracture toughness for Mode-I and Mode-II and improving the impact damage resistance. The work accomplished in this thesis will be followed with the following future work:

- Impact response of woven composites with ZnO nanowires reinforcement will be investigated at arctic temperatures (-60°C).
- Repeated impact of woven composites with ZnO nanowires reinforcement will be performed at room and arctic temperatures.

References

- [1] B. P. Justusson. *The Response of Textile Composites Subjected to Elevated Loading Rates*. PhD thesis, University of Michigan, 2015.
- [2] Bo. Madsen and E. K. Gamstedt. Wood versus plant fibers: Similarities and differences in composite applications. *Advances in Materials Science and Engineering*, 2013:564346, 2013.
- [3] T. Chou. *Microstructural Design of Fiber Composites*. Cambridge University Press, New York, 1992.
- [4] W. Roeseler, Branko Sarh, and M. Kismarton. Composite structures: The first 100 years. *16th International Conference on Composite Materials*, pages 1–10, 2013.
- [5] E. Barbero. *Introduction to Composite Materials Design*. Taylor & Francis, 6000 Broken Sound Parkway, 1 edition, 1998.
- [6] S. bagherpour. *Polyester*. InTech Prepress, Janeza Trdine 9, 51000 Rijeka, 1 edition, 2012.
- [7] A. Kaw. *Mechanics of Composite Materials*. Taylor & Francis Group, 6000 Broken Sound Parkway, 2 edition, 2006.
- [8] T. W. Clyne and P. J. Withers. *An Introduction to Metal Matrix Composites*. Cambridge University Press, 32 East 57th Street, 1 edition, 1993.
- [9] Department of Defense. *Composite Materials Handbook*, volume 5. MIL-HDBK-17-5, 2002.
- [10] E. J. Barbero. *Introduction to Composite Materials Design*. Taylor & Francis Group, 6000 Broken Sound Parkway, 2 edition, 2011.

- [11] ed. Miller, T. *Introduction to Composites*. Society of the Plastics Industry, New York, NY, 4 edition, 1998.
- [12] D. Hull and T. W. Clyne. *An Introduction to Composite Materials*. Cambridge University Press, 32 East 57th Street, 2 edition, 1996.
- [13] Encyclopedia of Polymer Science Engineering. John Wiley and Sons, New York, 1985.
- [14] D. Hull. *An Introduction to Composite Materials*. Cambridge University Press, 32 East 57th Street, 1 edition, 1981.
- [15] R.G. Budynas, J.K. Nisbett, and J.E. Shigley. *Shigley's mechanical engineering design*. McGraw-Hill series in mechanical engineering. McGraw-Hill, 2008.
- [16] D. B. Miracle and S. L. (ed.) Dinaldson. *ASM Handbook Volume 21: Composites*. 10 edition, 2010.
- [17] S. Lomov and I. Verpoest. *Textile Composite Materials: Polymer Matrix Composites.*, volume 9. John Wiley & Sons, New York, 2010.
- [18] P. Tan, L. Tong, and G. P. Steven. Modelling for predicting the mechanical properties of textile composites. *Composites Part A: Applied Science and Manufacturing*, 28(11):903–922, 1997.
- [19] 2d braided composites: A review for stiffness critical applications. *Composite Structures*, 85(1):43 – 58, 2008.
- [20] J. D. Skramstad. Evaluation of hand lay-up and resin transfer molding in composite wind turbine blade manufacturing. Master's thesis, Montana State University-Bozeman, 1999.
- [21] S.V. Hoa. *Principles of the Manufacturing of Composite Materials*. DEStech Publications, Incorporated, 2009.

- [22] P.K. Mallick. *Fiber-Reinforced Composites: Materials, Manufacturing, and Design, Third Edition*. Mechanical Engineering. CRC Press, 2007.
- [23] V. Kumar. Design and analysis of a compression molded carbon composite wheel center. Master's thesis, The University of Texas at Arlington, 2013.
- [24] U. Galan, Y. Lin, G. J. Ehlert, and H. Sodano. Effect of ZnO nanowire morphology on the interfacial strength of nanowire coated carbon fibers. *Composites Science and Technology*, 71(7):946–954, 2011.
- [25] S. Wicks, W. Wang, M. R. Williams, and B. L. Wardle. Multi-scale interlaminar fracture mechanisms in woven composite laminates reinforced with aligned carbon nanotubes. *Composite Science and Technology*, 100:128–135, 2014.
- [26] N. B. Adeyemi and K. N. Shivakumar. edlamination fracture toughness of woven-fabric composites under mixed-mode loading. *AIAA Journal*, 37(4):517–520, 1999.
- [27] K. S. Dransfield, K. J. Lalit, and Y. Mai. On the effects of stitching in CFRPs-I mode I delamination toughness. *Composite Science and Technology*, 58:815–827, 1998.
- [28] P. Robinson and S. Das. Mode-I dcb testing of composite laminates reinforced with z-direction pins: a simple model for the investigation of data reduction strategies. *Engineering Fracture Mechanics*, 71:345–364, 2003.
- [29] B. Ashrafi, J. Guan, and V. et. al. Mirjalili. Enhancement of mechanical performance of epoxy/carbon fiber laminate composites using single-walled carbon nanotubes. *Composite Science and Technology*, 3:1569–1578, 2011.
- [30] A. J. Smiley and R. B. Pipes. Rate effects on mode I interlaminar fracture toughness in composite materials. *Composite Materials*, 21:1–18, 1987.
- [31] D. Tenney, J. Davis, R. Byron, and N. Johnston. NASA composite materials development: Lessons learned and future challenges. *Conference Paper*, LF99-9370:1–58, 2009.

- [32] D. R. Bortz, C. Merino, and I. Martin-Gullon. Mechanical characterization of hierarchical carbon fiber/nanofiber composite laminates. *Composites: Part A*, 42:1584–1591, 2011.
- [33] B. Lars, J. Sumfleth, H. Hedemann, and K. Schulte. Improvement of fatigue life by incorporation of nanoparticles in glass fibre reinforced epoxy. *Composites: Part A*, 41:1419–1424, 2010.
- [34] A. Szekrenyes. Overview on the experimental investigations of the fracture toughness in composite materials. *Journal of Engineering materials and technology*, 100:1–19, 2011.
- [35] M. Czabaj and J. Ratcliffe. Comparison of intralaminar and interlaminar mode-I fracture toughness of unidirectional IM7/8552 graphite/epoxy composite. *Durability, Damage Tolerance, and Reliability Branch, NASA Langley Research Center.*, 2012.
- [36] A. Arguelles, J. Vina, A. F. Canteli, M. A. Castrillo, and Bonhomme. Interlaminar crack initiation and growth rate in a carbon-fibre epoxy composite under mode I fatigue loading. *Composites Science and Technology*, 68:2325–2331, 2008.
- [37] R. Khan, C. D. Rans, and R. Benedictus. Effect of stress ratio on delamination growth behavior in unidirectional carbon/epoxy under mode I fatigue loading. *Conference Paper, ICCM International Conferences on Composite Materials*:1–11, 2008.
- [38] K. O'Brian. Characterization of delamination onset and growth in a composite laminate. *NASA Technical Memorandum*, pages 1–63, 1981.
- [39] R. Rikards, F. G. Buchholz, A. K. Bledzki, G. Wacker, and Korjakin. Mode I, mode II and mixed-mode I/II interlaminar fracture toughness of gfrp influenced by fiber surface treatment. *Mechanics of Composite Materials*, 32:1–24, 1996.
- [40] S. Prasad, C.S. Venkatesha, and T. Jayaraju. Experimental methods of determining fracture toughness of fiber reinforced polymer composites under various loading condi-

tions. *Journal of Minerals & Materials Characterization & Engineering*, 10:1263–1275, 2011.

- [41] R. J Sager, P. J. Klein, D. C. Davis, D. C. Lagoudas, G. L. Warren, and H. Sue. Interlaminar fracture toughness of woven fabric composite laminates with carbon nanotube/epoxy interleaf films. *Wiley Online Library*, DOI 10.1002/app.33479:1–12, 2010.
- [42] K. Kong, B. K. Deka, M. Kim, A. Oh, H. Kim, Y. Park, and H. Park. Interlaminar resistive heating behavior of woven carbon fiber composite laminates modified with ZnO nanorods. *Composite Science and Technology*, 100:83–91, 2014.
- [43] Z. Fan, M. H. Santare, and S. G. Advani. Interlaminar shear strength of glass fiber reinforced epoxy composites enhanced with multi-walled carbon nanotubes. *Composites: Part A*, 9:540–34, 2008.
- [44] H. Qian, A. Bismarck, E. Greenhalgh, G. Kalinka, and Shaffer M. Hierarchical composites reinforced with carbon nanotube grafted fibers: the potential assessed at the single fiber level. *Chem Mater*, 95:1862–1869, 2008.
- [45] K. Kong, B. K. Deka, S. K. Kwak, A. Oh, H. Kim, Y. Park, and H. Park. Processing and mechanical characterization of ZnO polyester woven carbon-fiber composites with different ZnO concentrations. *Composites: Part A*, 555:152–160, 2013.
- [46] H. Hwang, M. Malakooti, B. Patterson, and H. Sodano. Increased interyarn friction through ZnO nanowire arrays grown on aramid fabric. *Composite Science and Technology*, 107:75–81, 2014.
- [47] J. B. Baxter and S. A. Eray. Nanowire-based dye-sensitized solar cells. *Applied Physics Letters*, 86(5):053114 1–3, 2005.
- [48] X. D. Wang, J. H. Song, J. Liu, and Z. L. Wang. Direct-current nanogenerator driven by ultrasonic waves. *Science*, 316:102–105, 2007.

- [49] Z. L. Wang and J. Song. Piezoelectric nanogenerators based on zinc oxide nanowire arrays. *Science*, 312:242–246, 2006.
- [50] Y. Lin, G. Ehlert, and H. Sodano. Increased interface strength in carbon fiber composites through ZnO nanowire interphase. *Advanced Functional Materials*, 19:2654–2660, 2009.
- [51] K. Chittajallu. Computational modeling of the vacuum assisted resin transfer molding (VARTM) process. *Thesis*, Clemson University, 2004.
- [52] S. Crook, H. Dhariwal, and G. Thornton. HREELS study of the interaction of formic acid with ZnO(1010) and ZnO(0001)-O. *Surface Science*, 382:19–25, 1997.
- [53] N. Dilsiz and J. P. Wightman. Surface analysis of unsized and sized carbon fibers. *Carbon*, 37:1105–1114, 1999.
- [54] N. Dilsiz and J. P. Wightman. Effect of acid-base properties of unsized and sized carbon fibers on fiber/epoxy matrix adhesion. *Colloids and Surfaces A: Physicochemical and Engineering Aspects*, 164:325–336, 2000.
- [55] R. Turgeman, O. Gershevit, M. Deutsch, B. M. Ocko, A. Gedanken, and C. N. Sukenik. Crystallization of highly oriented ZnO microrods on carboxylic acid-terminated SAMs. *Chem. Mater.*, 17:5048–5056, 2005.
- [56] G. J. Ehlert and H. Sodano. Development of a zinc oxide nanowire interphase for enhanced structural composites. *Doctoral Dissertation. Retrieved from: US National Library of Medicine National Institutes of Health*, pages 1–247, 2009.
- [57] Z. Hu, G. Oskam, and P. Searson. Influence of solvent on the growth of ZnO nanoparticles. *Journal of Colloid and Interface Science*, 263:545–460, 2003.
- [58] M. Law, L. E. Greene, J. C. Johnson, R. Saykally, and P. Yang. Nanowire dye-sensitized solar cells. *Nature Materials*, 4:455–459, 2005.

- [59] Y. Wang and J. G. Williams. Corrections for mode-II fracture toughness specimens of composite materials. *Composites Science and Technology*, 43:251–256, 1992.
- [60] H. Yoshihara. Mode II initiation fracture toughness analysis for wood obtained. *Composites Science and Technology*, 65:2198–2207, 2005.
- [61] A B. Pereira, A B. De Morais, A T. Marques, and P T. Castro. Mode II interlaminar fracture of glass/epoxy multidirectional laminates. *Composites Part A: Applied Science and Manufacturing*, 35(2):265–272, 2004.
- [62] P. N. B. Reis, J. A. M. Ferreira, J. D. M. Costa, and A. M. Pereira. Interlaminar fracture in woven carbon/epoxy laminates. *Frattura ed Integrita Strutturale*, 30:431–437, 2014.
- [63] ASTM International. Standard test method for mode I interlaminar fracture toughness of unidirectional fiber-reinforced polymer matrix composites. *D5528 13*, pages ASTM International, West Conshohocken, PA, DOI: 10.1520/D5528, www.astm.org., 2013.
- [64] ASTM International. Standard test method for mode II interlaminar fracture toughness of unidirectional fiber-reinforced polymer matrix composites. *D7905/D7905M-14*, pages 1–18, 2014.
- [65] Y. Zhu. Characterization of interlaminar fracture toughness of a carbon/epoxy composite material. Master’s thesis, The Pennsylvania State University, 2009.
- [66] A. Julias and V. Murali. Effect of carbon fiber position on the impact behavior of glass/carbon fiber hybrid composite laminates. *International Journal of Applied Engineering Research*, 9(26):9103–9106, 2014.
- [67] S.N.A. Safri, M.T.H. Sultan, N. Yidris, and F. Mustapha. Low velocity and high velocity impact test on composite materials - a review. *International Journal of Engineering and Science*, 3(9):50–60, 2014.

- [68] P. Sjoblom. Simple design approach against low velocity impact damage. *Proc. 32 SAMPE Symposium*, (Anaheim, CA):30–52, 1987.
- [69] K.N Shivakumar, W. Elber, and W. Illg. Prediction of impact force and duration due to low velocity impact on circular composite laminates. *Journal of Applied Mechanics*, 52:674–680, 1985.
- [70] W.J. Cantwell and J. Morton. Impact perforation of carbon-fiber reinforced plastics. *Composites Science and Technology*, 38:119–141, 1990.
- [71] S. Abrate. Impact on laminated composites: Recent advances. *Applied Mechanics Reviews*, 47(11):517–544, 1994.
- [72] V. Caprino, V. Lopresto, C. Scarponi, and G. Briotti. Effect of ZnO nanowire morphology on the interfacial strength of nanowire coated carbon fibers. *Composites Science and Technology*, 59:2279–2286, 1999.
- [73] R. Karakuzu, E. Erbil, and A. Mehmet. Impact characterization of glass/epoxy composite plates: An experimental and numerical study. *Composites: Part B*, 41:388–395, 2010.
- [74] J-K Kim and M-L. Sham. Impact and delamination failure of woven-fabric composites. *Composite Science Technology*, 60:745–61, 2000.
- [75] T-W. Shyr and Y-H. Pan. Impact resistance and damage characteristic of composite laminates. *Composite Structures*, 62:193–203, 2003.
- [76] S. Babu and H. K. Shivanand. Impact analysis of laminated composite on glass fiber and carbon fiber. *International Journal of Emerging Technology and Advanced Engineering*, 4(6):824–829, 2014.
- [77] M.S. Sohn and X.Z. Hu. Processing of carbon-fibre/epoxy composites with cost-effective interlaminar reinforcement. *Composite Science and Technology*, 58:211–220, 1998.

- [78] A.G. Castellanos, Md. S. Islam, M.A.I Shuvo, Y. Lin, and P. (in press) Prabhakar. Nanowire reinforcement of woven composites for enhancing interlaminar fracture toughness. *Journal of Sandwich Structures and Materials*, Advance online publication:doi:, 2016.
- [79] ASTM International. Standard test method for measuring the damage resistance of a fiber-reinforced polymer matrix composite to a drop-weight impact event. *D7136/D7136M-15*, pages 1–16, www.astm.org., 2015.
- [80] G. Belingardi and R. Vadori. Influence of the laminate thickness in low velocity impact behavior of composite material plate. *Composiite Structures*, 61:27–38, 2003.

Curriculum Vitae

Alejandra Castellanos was born on February 8, 1991. She was born in Ciudad Juarez, Chihuahua, Mexico. She started college at the University of Texas at El Paso in the fall of 2009. There she worked as peer leader and undergraduate Research Assistant while pursuing her bachelors degree in Mechanical Engineering. At the completion of the degree, she was recognized for being part of the top ten mechanical engineering students and was graduated with Magna Cum Laude.

In fall 2014, she entered the Graduate School at the University of Texas at El Paso, where she has earned a Masters degree in Mechanical Engineering. There she worked as a Teaching and Research Assistant while pursuing her masters degree. Her research interests are focused on impact damage tolerance and durability of sandwich composites in extreme conditions. She has published and presented papers at conferences. Besides, Alejandra Castellanos has been awarded by the department of Mechanical Engineering at the University of Texas at El Paso as the most outstanding Graduate student in 2016 and has been selected as the Graduate Student Marshal of Students from the College of Engineering.

Permanent address: 3225 Scarlet Point Dr.

El Paso, Texas 79938